



HAL
open science

Europe-wide atmospheric radionuclide dispersion by unprecedented wildfires in the Chernobyl Exclusion Zone, April 2020

Olivier Masson, Oleksandr Romanenko, Olivier Saunier, Serhii Kirieiev, Valentyn Protsak, Gennady Laptev, Oleg Voitsekhovych, Vanessa Durand, Frederic Coppin, Georg Steinhauser, et al.

► To cite this version:

Olivier Masson, Oleksandr Romanenko, Olivier Saunier, Serhii Kirieiev, Valentyn Protsak, et al.. Europe-wide atmospheric radionuclide dispersion by unprecedented wildfires in the Chernobyl Exclusion Zone, April 2020. *Environmental Science and Technology*, 2021, 55 (20), pp.13834-13848. 10.1021/acs.est.1c03314 . hal-03462522

HAL Id: hal-03462522

<https://hal.science/hal-03462522>

Submitted on 1 Dec 2021

HAL is a multi-disciplinary open access archive for the deposit and dissemination of scientific research documents, whether they are published or not. The documents may come from teaching and research institutions in France or abroad, or from public or private research centers.

L'archive ouverte pluridisciplinaire **HAL**, est destinée au dépôt et à la diffusion de documents scientifiques de niveau recherche, publiés ou non, émanant des établissements d'enseignement et de recherche français ou étrangers, des laboratoires publics ou privés.

Europe-wide atmospheric radionuclide dispersion by unprecedented wildfires in the Chernobyl Exclusion Zone, April 2020

Olivier Masson^{1*}, Oleksandr Romanenko², Olivier Saunier¹, Serhii Kirieiev³, Valentin Protsak⁴, Gennady Laptev⁴, Oleg Voitsekhovych⁴, Vanessa Durand¹, Frédéric Coppin¹, Georg Steinhauser⁵, Anne de Vismes Ott¹, Philippe Renaud¹, Damien Didier¹, Béatrice Boulet¹, Maxime Morin¹, Miroslav Hýža⁶, Johan Camps⁷, Olga Belyaeva⁸, Axel Dalheimer⁹, Konstantinos Eleftheriadis¹⁰, Catalina Gascó-Leonarte¹¹, Alexandra Ioannidou¹², Krzysztof Isajenko¹³, Tero Karhunen¹⁴, Johan Kastlander¹⁵, Christian Katzlberger¹⁶, Renata Kierepko¹⁷, Gert-Jan Knetsch¹⁸, Júlia Kövendiné Kónyi¹⁹, Jerzy Wojciech Mietelski¹⁷, Michael Mirsch⁹, Bredo Møller²⁰, Jelena Krmeta Nikolić²¹, Pavel Peter Povince²², Rosella Rusconi²³, Vladimir Samsonov²⁴, Ivan Sýkora²², Elena Simion²⁵, Philipp Steinmann²⁶, Stylianos Stoulos¹², José Antonio Suarez-Navarro¹¹, Herbert Wershofen²⁷, Daniel Zapata-García²⁷, Benjamin Zorko²⁸

1 Institut de Radioprotection et de Sûreté Nucléaire (IRSN), Fontenay-Aux-Roses, 92260, France, olivier.masson@irsn.fr

2 Rivne Nuclear Power Plant (ENERGOATOM), Varash, Rivne Region, 34400, Ukraine

3 State Specialized Enterprise Ecocentre (SSE ECOCENTRE), Chornobyl, Kiev region, 07270, Ukraine

4 Ukrainian Hydrometeorological Institute (UHMI), Kyiv, 03028, Ukraine

5 Institute of Radioecology and Radiation Protection, Leibniz Universität Hannover, Hannover, 30419, Germany

6 National Radiation Protection Institute (SÚRO), Prague 4, 140 00, Czech Republic

7 StudieCentrum voor Kernenergie - Centre d'Etude de l'Energie Nucléaire (SCK-CEN), 2400, Mol, Belgium

8 Center for Ecological-Noosphere Studies (NAS RA), Department of Radioecology, 0025 Yerevan, Armenia

9 Deutscher Wetterdienst (DWD), 63067 Offenbach, Germany

10 Institute of Nuclear and Radiological Sciences & Technology, Energy & Safety, National Centre for Scientific Research "Demokritos", Athens, 15310, Greece

11 Centro de Investigaciones Energéticas, Medioambientales y Tecnológicas (CIEMAT), Unidad de Radioactividad Ambiental y Vigilancia Radiológica, Madrid, 28040, Spain

12 Aristotle University of Thessaloniki, Nuclear Physics and Elementary Particle Physics Division, Physics Department, Thessaloniki, 54124, Greece

13 Central Laboratory for Radiological Protection (CLRP), Warsaw, PL 03-194, Poland

14 Radiation and Nuclear Safety Authority (STUK), PL 14, Helsinki, 00881, Finland

15 Swedish Defence Research Agency (FOI), 164 90 Stockholm, Sweden

16 Austrian Agency for Health and Food Safety (AGES), Department of Radiation Protection and Technical Quality Assurance, Vienna, 1220, Austria

17 The Henryk Niewodniczanski Institute of Nuclear Physics (IFJ), Polish Academy of Sciences, Kraków, 31-342, Poland

18 National Institute of Public Health and the Environment (RIVM), PO Box 1, Bilthoven, NL-3720 BA, The Netherlands

19 National Public Health Center, Department of Radiobiology and Radiohygiene (NNK SSFO), Budapest, H-1221, Hungary

20 Norwegian Radiation and Nuclear Safety Authority (DSA), Emergency Preparedness and Response, Svanvik, NO-9925, Norway

21 Vinča Institute of Nuclear Sciences, Department of Radiation and Environmental Protection, Belgrade, 11351, Serbia

22 Department of Nuclear Physics and Biophysics, Comenius University, Bratislava, 842 48, Slovakia

23 Centro Regionale Radioprotezione, Agenzia Regionale per la Protezione dell'Ambiente della Lombardia (ARPA Lombardia), 20124 Milan, Italy

24 National Center for Hydrometeorology, Radioactive Contamination Control, and Environmental Monitoring (BELHYDROMET), Minsk, 220114, Belarus

25 National Environmental Protection Agency (NEPA), National Reference Laboratory, Bucharest, 060031, Romania

26 Federal Office of Public Health (FOPH - OFSP), Environmental Radioactivity Section, Liebefeld, CH-3097, Switzerland

27 Physikalisch-Technische Bundesanstalt (PTB), Braunschweig, 38116, Germany

28 Institut "Jozef Stefan" (IJS), SI-100 Ljubljana, Slovenia

Keywords : Wildfire, radionuclides, Chernobyl, firefighters, dose assessment

1 **Abstract**

2 From early April 2020, wildfires raged in the highly contaminated areas around the Chernobyl nuclear
3 power plant (CNPP), Ukraine. For about four weeks, the fires spread around and into the Chernobyl
4 exclusion zone (CEZ) and came within a few kilometres of both the CNPP and radioactive waste storage
5 facilities. Wildfires occurred on several occasions throughout the month of April. They were extinguished,
6 but weather conditions and the spread of fires by airborne embers and smoldering fires led to new fires
7 starting at different locations of the CEZ. The forest fires were only completely under control at the
8 beginning of May, thanks to the tireless and incessant work of the firefighters and a period of sustained
9 precipitation. In total, 0.7-1.2 TBq ^{137}Cs were released into the atmosphere. Smoke plumes partly spread
10 south and west and contributed to the detection of airborne ^{137}Cs over the Ukrainian territory and as far away
11 as Western Europe. The increase in airborne ^{137}Cs ranged from several hundred $\mu\text{Bq}\cdot\text{m}^{-3}$ in northern Ukraine
12 to trace levels of a few $\mu\text{Bq}\cdot\text{m}^{-3}$ or even within the usual background level in other European countries.
13 Dispersion modeling determined the plume arrival time and was helpful in the assessment of the possible
14 increase in airborne ^{137}Cs concentrations in Europe. Detections of airborne ^{90}Sr (emission estimate 345 –
15 612 GBq) and Pu (up to 75 GBq, mostly ^{241}Pu) were reported from the CEZ. Americium-241 represented
16 only 1.4% of the total source term corresponding to the studied anthropogenic radionuclides but would have
17 contributed up to 80% of the inhalation dose.

18 **Synopsis**

19 Wildfires in highly radioactive environment can re-emit radionuclides into the atmosphere. Such emissions
20 present a potential health risk for firefighters.

21 **Introduction**

22 As a result of global fallout from atmospheric nuclear explosions and the Chernobyl nuclear accident, the
23 Eurasian boreal forest represents one of the greatest stocks of long-lived anthropogenic radionuclides in the
24 terrestrial environment, primarily ^{137}Cs ($T_{1/2} = 30.1$ yr.).¹ Since large wildfires in 1992, the fire hazard in the
25 Chernobyl area has been viewed with serious concern.² These fire events are capable of emitting
26 radionuclides (RN) into the atmosphere and can redistribute part of the already deposited RN.³ These RN
27 are found in topsoil layers, forest litter, and in the biomass. Emission of natural RN such as ^{210}Po are also
28 known to occur from wildfire events.^{4,5} Wildfires in heavily contaminated areas generate radioactive smoke
29 particles and thus an additional radiation exposure through inhalation or ingestion of contaminated
30 foodstuff, following RN re-deposition.⁶ The consequences of wildfires in the highly contaminated area
31 around the CNPP (parts of northern Ukraine, southern Belarus and the western part of the Russian
32 Federation) as well as emission factors or resuspension factors have already been investigated at a local

33 level.⁷⁻¹² Evidence for long-range transport of RN from fires on an international scale is more recent.^{1, 13}
34 Considerable efforts have been made by Ukraine, Belarus, and the Russian Federation to limit the
35 consequences of fires in contaminated areas.^{14, 15} However, despite preventative measures (e.g., controlled
36 fires, fire-breaks, access trails, limitation of fuel quantities in some areas, minimization of human presence)
37 intended to limit both ignition and the spread of wildfires, they occur on a yearly basis in the Chernobyl
38 area^{16, 17} and affect wildlife.¹⁸ The Chernobyl ecosystem has regularly suffered from major wildfires notably
39 in 1992, 1999, 2000, 2002-2004, 2006, 2010, 2015, 2016, and 2018^{15, 19} with major impacts on the
40 vegetation cover.²⁰ For a brief historic review of wildfires in contaminated areas, see the Supporting
41 Information (SI).

42
43 Herein, we investigate the devastating April 2020 wildfires, which lasted for about four weeks in the
44 Ukrainian part of the contaminated areas around the CNPP. The detailed geographic analysis and timeline
45 is provided in the SI. The fire situation in the CEZ and bordering areas was characterized by a combination
46 of numerous ignitions and subsequent spread of fires. Their magnitude varied according to different
47 parameters: 1) biomass type, vegetation density, and location accessibility (forest, meadow, peatland, and
48 marshland); 2) meteorological parameters (wind speed, wind direction, precipitation frequency and
49 amount). These multiple factors hindered firefighting, despite the mobilization of nearly 400 firefighters
50 and 90 specialized aerial and terrestrial vehicles (two AN-32P airplanes, one Mi-8 water-bombing
51 helicopter, heavy engineering equipment, and seven additional road construction machines of the Armed
52 Forces of Ukraine). The first three weeks of April saw the development of particularly large and numerous
53 fires. Two main fire areas were identified during this period: in the Polisske district and in the Kopachi-
54 Chistogalovka-CNPP cooling pond (<12 km from CNPP). Daily information about burned areas including
55 vegetation cover, contamination density, and radionuclide emissions were then published by the Ukrainian
56 Hydrometeorological Institute (UHMI).²¹ According to the UHMI, 870 km² were burned in total, including
57 65 km² in proximity to the CNPP and 20 km² on the left bank of the Pripyat river.

58 Because of a period of easterly and southerly winds, slight increases in the airborne ¹³⁷Cs were observed at
59 a few western European locations while most of the airborne ¹³⁷Cs concentrations remained within the
60 μBq·m⁻³ range on a weekly sampling basis, which corresponds to the usual background level. Such western
61 detections are somewhat rare since the general air mass circulation is usually easterly. A similar situation
62 had already occurred from the end of August to early September 2002 with a slight increase in airborne
63 ¹³⁷Cs concentrations in the western European atmosphere.²² The follow-up of the April 2020 wildfire
64 situation was scrutinized on a daily basis by the UHMI,²¹ and regularly commented by the SCK-CEN^{23, 24}
65 and the IRSN.²⁵⁻²⁸ In total about 1,100 ¹³⁷Cs results were gathered throughout Europe including already
66 published data from the International Monitoring System (IMS) in support to the Comprehensive Nuclear-

67 Test-Ban Treaty Organization.^{23, 24} This collection, which also includes a hundred values for ⁹⁰Sr, ²³⁸Pu and
68 ²³⁹⁺²⁴⁰Pu from Ukraine, corresponds to the most comprehensive available dataset related to that event (see
69 Tables S6 and S7, SI). The purpose of this study is to investigate both the RNs source terms and the
70 additional exposure to RNs for firefighters and inhabitants of Kiev. Part of these assessments are based on
71 numerous measurements performed during this event and dispersion calculation. RNs that were not
72 determined have been estimated based on RN ratios typical of the Chernobyl accident and ²¹⁰Po results
73 obtained during other wildfires.

74

75 **Background**

76 Starting on April 26, 1986 and for a period of ten days, the Chernobyl accident released harmful quantities
77 of radionuclides of I, Cs, Te, Sr, Pu, and others (see Table S1, SI). Some regions of Belarus, Ukraine and
78 the Russian Federation were seriously affected by the radioactive fallout from the CNPP accident.²⁹ About
79 6 million ha of forest including 2.5 million ha in Ukraine were heavily contaminated. In the most
80 contaminated regions following the accident the dominant forests were young or middle-aged pine and pine-
81 hardwood stands, with a high fire risk.⁸ The highest radionuclide deposition density occurred in the area
82 surrounding the CNPP, in the so-called Chernobyl Exclusion Zone (CEZ) in Ukraine and in the Polesie
83 State Radioecological Reserve (PER) in Belarus. The CEZ, initially about 30 km in radius around the CNPP
84 was subsequently enlarged to an oblong area of 2,600 km² with a 439 km circumference. It is located
85 approximately 100 km north of Kiev (see Figure S1, SI). The CEZ is mostly covered by forest where
86 radionuclides are distributed between soil, forest litter, and vegetation. Between 57 and 79% of the total
87 ¹³⁷Cs contamination is stored within the upper soil layer (0- 2 cm).³⁰ Only a few percent of the ¹³⁷Cs
88 inventory is contained in the living biomass, where ¹³⁷Cs behaves like potassium, its chemical analogue.
89 During fire events in forested areas, the main source of radioactive aerosols is the burning forest litter. In
90 comparison, the trees affected by the fire emit minor amounts of ¹³⁷Cs and ⁹⁰Sr and only trace amounts of
91 Pu isotopes and ¹⁴⁴Ce.^{31, 32} More information about radionuclide apportionment in the terrestrial ecosystem
92 and fire impact is provided in the SI.

93 Present day contamination is the result of radionuclides released during the accident with a medium or long
94 radioactive half-life [¹³⁷Cs (T_{1/2} = 30.07 yr.), ⁹⁰Sr (T_{1/2} = 29.14 yr.), ²³⁸Pu (T_{1/2} = 87.76 yr.), ²³⁹Pu (T_{1/2} =
95 24.13 10³ yr.), ²⁴⁰Pu (T_{1/2} = 6.57 10³ yr.), ²⁴¹Pu (T_{1/2} = 14.35 yr.) and those arising as decay products of them:
96 ²⁴¹Am (T_{1/2} = 432 yr., ²³⁷Np (T_{1/2} = 2.144 10⁶ yr.)]. Conversely to ¹³⁷Cs which spread and deposited all over
97 Europe, ⁹⁰Sr, and Pu isotopes as nuclear fuel debris were mainly deposited in Ukraine and Belarus.³³
98 Cesium-137 is the preferred RN used in forecasting the long-term radiological consequences after an

99 accidental release, because of its radiotoxicity, bioaccumulation, comparatively long half-life and
100 straightforward measurement procedure.

101 Once forests become contaminated with radiocesium, any further significant redistribution is limited.
102 Processes of small scale redistribution include resuspension, fire and erosion/runoff.³ According to the
103 International Atomic Energy Agency (IAEA), none of these processes are likely to result in any significant
104 migration of radiocesium beyond the location of initial deposition.³⁴ The question of radionuclide
105 redistribution may be a matter of interest for nearest adjacent areas that would have not been initially
106 contaminated or with a much lower contamination of their ecosystem. This gives interest for radionuclide
107 redistribution on a local scale and detection of trans-border fire plumes. Depending on the wildfire intensity,
108 smoke plumes may reach atmospheric layers up to several kilometres above ground level and travel for
109 thousands of kilometers¹, or be maintained in the atmosphere up to about 20 days.³⁵ Previous studies have
110 already brought some reassuring general information.³⁶ Over already contaminated areas the additional
111 contamination due to redistribution of artificial radionuclides by a fire remains low, about 1% of the previous
112 inventory.³² Thanks to atmospheric dispersion and buoyancy effects, a sharp decrease in the airborne
113 concentration can be expected with distance (a dozen fold less at a distance of 100 m and thousands fold
114 less at a distance of several kilometres from the fire line.^{32, 37} Regarding the redistribution or loss of RNs
115 from a burned area, it has been suggested that a wildfire outbreak might export at least 40% and up to 90%
116 of the ¹³⁷Cs inventory.⁷⁻¹² In other words, this would mean that a fire could virtually “clean” an area from
117 ¹³⁷Cs. Current and historical research does not in any way support this proposition.

118 In several studies, it has been tried to determine the proportion of radionuclides that can be emitted into the
119 atmosphere from a zone with a given contamination density or emitted from burning material during a fire,
120 either through a resuspension factor K (m^{-1}) or an emission factor E_f (%). A compilation of both parameters
121 can be found in the SI. The UHMI calculated estimates of radionuclide emission into the atmosphere daily.
122 Their estimates relied on detailed satellite observations of the extent of the fires and combined the specific
123 contamination density of the burned areas, the vegetation type, and the specific radionuclide distribution in
124 the ecosystem. For the April 2020 fire event, the UHMI used a ¹³⁷Cs emission factor of 5% because of the
125 exceptional intensity of the crown fires. As of April 20, a total of 690 GBq of ¹³⁷Cs would have been released
126 into the atmosphere.²¹ The ¹³⁷Cs source term was later re-evaluated including emission from April 20 to 30,
127 leading to a release between 600 and 860 GBq for the CEZ, as well as 60 to 85 GBq for the Zhytomyr
128 region.³⁰ Additionally, 13.5 GBq of ⁹⁰Sr and 0.059 GBq of Pu isotopes were estimated by the UHMI to have
129 been released during fires. Using a similar approach (satellite observations of fire spots, burned areas,
130 emission factors), Evangelidou & Eckhardt estimated that 341 GBq of ¹³⁷Cs, 51 GBq of ⁹⁰Sr, 2 GBq of ²³⁸Pu,
131 0.033 GBq of ²³⁹Pu, 0.066 GBq of ²⁴⁰Pu and 0.504 GBq of ²⁴¹Am were released between April 1 – 22,
132 2020.³⁸

133

134 **Plume detection in Ukraine**

135 Plume detection was revealed by a 1,000 to 10,000-fold ^{137}Cs increase (i.e. up to a fraction of a $\text{Bq}\cdot\text{m}^{-3}$ in
136 the CEZ and up to a fraction of a $\text{mBq}\cdot\text{m}^{-3}$ in the Kiev area) as compared to the usual ^{137}Cs average
137 background levels of about $3.5 \text{ mBq}\cdot\text{m}^{-3}$ in the CEZ and $6 \mu\text{Bq}\cdot\text{m}^{-3}$ in Kiev.³² Levels in excess of critical
138 threshold concentrations (i.e. a reference level of $0.21 \text{ mBq}\cdot\text{m}^{-3}$ for ^{137}Cs in Ukraine) were observed in
139 proximity to fire lines, owing to wildfire magnitude. High airborne contamination values were observed due
140 to the proximity of aerosol samplers with the fire lines (i.e. $42 \text{ mBq}\cdot\text{m}^{-3}$ on April 12 at the Korogodske
141 forestry “square 11” station). An even higher ^{137}Cs value of $180 \text{ mBq}\cdot\text{m}^{-3}$ ($0.18 \text{ Bq}\cdot\text{m}^{-3}$) was momentarily
142 reported on April 13 at the CNPP “Ukrenergomontazh - Open SwitchGear-750 point”, at about 500 m from
143 the damaged reactor. Such orders of magnitude were similar to those reported during previous wildfire
144 outbreaks: $250 \text{ mBq}\cdot\text{m}^{-3}$ at the end of June, 2015 near the abandoned village of Polis’ke, $150 \text{ mBq}\cdot\text{m}^{-3}$ on
145 July 29, 2016 in the “Red forest”, $25 \text{ mBq}\cdot\text{m}^{-3}$ on June 29, 2017 in the CEZ, too.^{39, 40} During the April 2020
146 fires, the UHMI estimated that the additional ground surface ^{137}Cs deposition in the CEZ peaked at about
147 $65 \text{ Bq}\cdot\text{m}^{-2}$ where the surface contamination was already in the $\text{MBq}\cdot\text{m}^{-2}$ to the tens of $\text{MBq}\cdot\text{m}^{-2}$ range (pers.
148 comm., O. Voitsekhovych, UHMI).

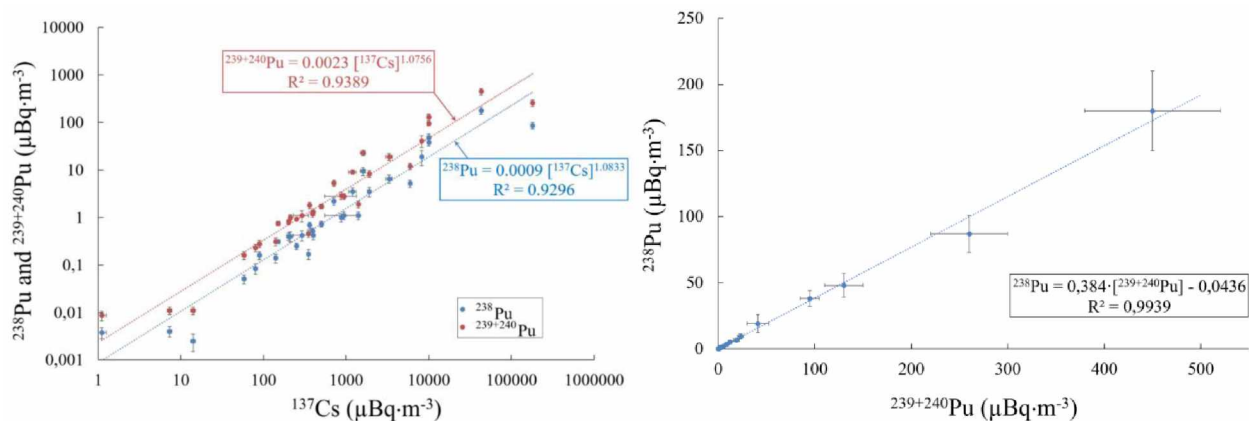
149 Strontium-90 was also detected in up to 20 locations, all of them in the highly contaminated area (see Table
150 S7, SI). Based on about 40 pairs of ^{137}Cs and ^{90}Sr measurements, the $^{90}\text{Sr}/^{137}\text{Cs}$ activity ratio exhibited such
151 a significant variation (0.04 – 6.67) that it could not reasonably be represented by an aggregated statistic
152 (average value of 0.91). Hereafter, the highest ratio (6.67) was considered as an outlier and hence not taken
153 into account as representative of the whole fire situation. It corresponded to the pair of ^{137}Cs and ^{90}Sr values
154 that were by far the highest (as reported on April 13 from the OSG-750 station with $^{137}\text{Cs}=180 \text{ mBq}\cdot\text{m}^{-3}$ and
155 $^{90}\text{Sr}=1,200 \text{ mBq}\cdot\text{m}^{-3}$) and because these concentrations were obtained over a very short period of time (~half
156 an hour). 80% of the $^{90}\text{Sr}/^{137}\text{Cs}$ ratios were less than or equal to 1. Inversely, 20% of airborne ^{90}Sr
157 concentrations were higher than ^{137}Cs . This suggests that ^{90}Sr and ^{137}Cs biomass contamination levels and
158 magnitude of the fires were much more likely to be of significance in the observed $^{90}\text{Sr}/^{137}\text{Cs}$ ratio.
159 Measurements performed using aerosol impactors (Yoschenko et al.) showed in general that ^{90}Sr bound to
160 coarse particles with an activity median aerodynamic diameter (AMAD) of $> 25 \mu\text{m}$, while ^{137}Cs
161 predominantly bound to the finer aerosol fraction.³² Therefore, it is likely that the largest part of ^{90}Sr
162 emissions remained airborne for only 1 – 2 km. The distance between mobile aerosol sampling units and
163 the fire line thus participated to the variability of the $^{90}\text{Sr}/^{137}\text{Cs}$ ratio.

164 Contrarily to ^{90}Sr which behaves like calcium (a factor of main influence on the plant physiology), ^{137}Cs is
165 much less bioaccumulated in wood.¹⁸ Recently, Holiaka et al.⁴¹ have reported a rather constant average ^{90}Sr

166 /¹³⁷Cs ratio of about 2.5 in wood disks of Scots Pine stems sampled approximately 5 km north of the CNPP.
 167 This value is clearly different from that found on average in aerosols (0.76, range 0.04 – 3.1) during the
 168 April wildfires. However, when looking into detail to the radial distribution of ¹³⁷Cs and ⁹⁰Sr in the wood
 169 disks the authors concluded that, due to the year-by-year root uptake increase, a newly formed annual ring
 170 receives a bigger amount of radiocesium than a ring formed in the previous years. In addition, ¹³⁷Cs is also
 171 translocated into these rings from older sapwood.⁴¹ Conversely, the radial distribution of ⁹⁰Sr shows
 172 decreasing concentrations from heartwood to sapwood, i.e. decreasing ⁹⁰Sr concentrations from inner to
 173 outer parts.⁴¹ The lower ⁹⁰Sr /¹³⁷Cs ratio observed in aerosols could thus be consistent with a partial
 174 combustion of aged tree trunks which remain charred after the fire goes through while the outer parts of the
 175 tree (peripheral annual rings with a lower ⁹⁰Sr /¹³⁷Cs ratio) are burned.

176
 177 In addition to ¹³⁷Cs and ⁹⁰Sr, about thirty measurements for both airborne ²³⁸Pu and ²³⁹⁺²⁴⁰Pu were reported
 178 from the CEZ (see Table S7, SI). Maximum values for hourly measurements reached 180 μBq·m⁻³ for ²³⁸Pu
 179 and 450 μBq·m⁻³ for ²³⁹⁺²⁴⁰Pu on April 12 at the Korohodske forestry monitoring station. The average
 180 ²³⁸Pu/²³⁹⁺²⁴⁰Pu ratio found was 0.40, which is slightly lower than the value of 0.48 - 0.50 reported during the
 181 Chernobyl accident in 1986 or 0.47 found by Kashparov et al.⁴²⁻⁴⁴ for the residual contamination of the
 182 environment in 2000. The ²³⁸Pu/¹³⁷Cs, ²³⁹⁺²⁴⁰Pu/¹³⁷Cs and ²³⁸Pu/²³⁹⁺²⁴⁰Pu relationships shown in Figure 1 are
 183 those that will be used hereafter in source term assessments.

184



185
 186 Figure 1: (Left) Airborne ²³⁸Pu and ²³⁹⁺²⁴⁰Pu vs. ¹³⁷Cs concentrations in the CEZ, Ukraine, April 2020.
 187 (Right) Airborne ²³⁸Pu concentration vs. ²³⁹⁺²⁴⁰Pu concentration in aerosols sampled in the CEZ, April 2020.
 188

189 Except close to the fire spreading in the CEZ where the gamma dose equivalent rate was in the 0.5 -
 190 30 μSv·h⁻¹ range, the highest airborne concentrations measured elsewhere in Ukraine were not high enough
 191 to significantly increase the ambient gamma dose equivalent rate. Daily average airborne ¹³⁷Cs
 192 concentrations measured by the UHMI in Kiev reached 290 μBq·m⁻³ from April 8 to 9 and up to 700 μBq·m⁻³

193 from April 10 to 11. The maximum observed average value during each daily sampling period remained far
194 below the National Radiation Safety Standards of Ukraine⁴⁵ establishing the allowed concentration of ¹³⁷Cs
195 to 800 mBq·m⁻³. Such concentration increases were concomitant with the smoke plume arrival in Kiev and
196 have to be compared with the yearly average local background concentration of 6 μBq·m⁻³ (usual range 3 –
197 8 μBq·m⁻³).

198

199 **Plume detection outside Ukraine**

200 All the positive airborne ¹³⁷Cs measurements outside Ukraine during April 2020 were in the μBq·m⁻³ range,
201 i.e. within or just above the typical background ¹³⁷Cs level usually observed in the springtime (see Table S6,
202 SI). The reason for this background and the low-level airborne ¹³⁷Cs persistence is examined in the
203 Supporting Information. Considering the airborne ¹³⁷Cs background routinely observed and resulting from
204 resuspension on a local scale, it was difficult to assert if the measured concentrations in april 2020 included
205 a tiny and remote fire contribution. For instance, a weekly average value of $5.67 \pm 0.58 \mu\text{Bq}\cdot\text{m}^{-3}$ was
206 observed at Seehausen in north-eastern Germany (52.891 N ; 11.729 E). This value is significantly higher
207 than the airborne level in the westernmost Europe. However, it remains in the usual range of variability as
208 a result of a comparatively more significant local Chernobyl deposition in 1986. In addition, Seehausen is
209 also known for ¹³⁷Cs resuspension during periods of dry meteorological conditions (Pers. Comm. A.
210 Dalheimer, DWD). Moreover, dispersion calculation did not reveal a noticeable transportation of airborne
211 ¹³⁷Cs to Germany. It means that this location was not affected by the fire plume. In Norway, positive ¹³⁷Cs
212 detections were observed at the two northernmost sampling locations (Viksjo fjell, 69.62 N ; 30.72 E) and
213 Svanhovd (69.45 N ; 30.04 E) with very low ¹³⁷Cs concentrations (< 1 μBq·m⁻³). However, because of a
214 persistent snow cover prone to prevent ¹³⁷Cs resuspension from soil both on a local and regional scales, it
215 can be stated that airborne ¹³⁷Cs were mostly related to forest fires in Ukraine, as suggested by the
216 coincidence between simulation of plume arrival and sampling dates with higher than usual airborne ¹³⁷Cs
217 concentration (see *Plume dispersion analysis* section). Contrarily to what was first expected, in Eastern
218 Europe and relatively close to Ukraine, the fire plume, although more concentrated than in Western Europe,
219 did not ensue a significant ¹³⁷Cs increase above the usual local or regional ¹³⁷Cs background level which is
220 usually also higher than in Western Europe. At some Eastern Europe locations, the weekly average ¹³⁷Cs
221 activity may have hidden the peak value that would have been found if the sampling period had coincided
222 with the sampling duration. In such case, the atmospheric dispersion modeling is the only way to retrieve
223 this information (see *Plume dispersion analysis* section). For instance, in Budapest, it is estimated that the
224 smoke plume arrived between April 5 and 6 and remained until April 9. A ¹³⁷Cs peak value of about
225 25 μBq·m⁻³ was assessed. This peak cannot be foreseen based on the weekly-average sampling value
226 (12.8 μBq·m⁻³). In Poland, the estimated ¹³⁷Cs peak value was about 50 μBq·m⁻³ while the corresponding

227 weekly average value was at most about $6 \mu\text{Bq}\cdot\text{m}^{-3}$ which is not much higher than the usual ^{137}Cs background
228 level ranging from less than $1 \mu\text{Bq}\cdot\text{m}^{-3}$ to a few $\mu\text{Bq}\cdot\text{m}^{-3}$.

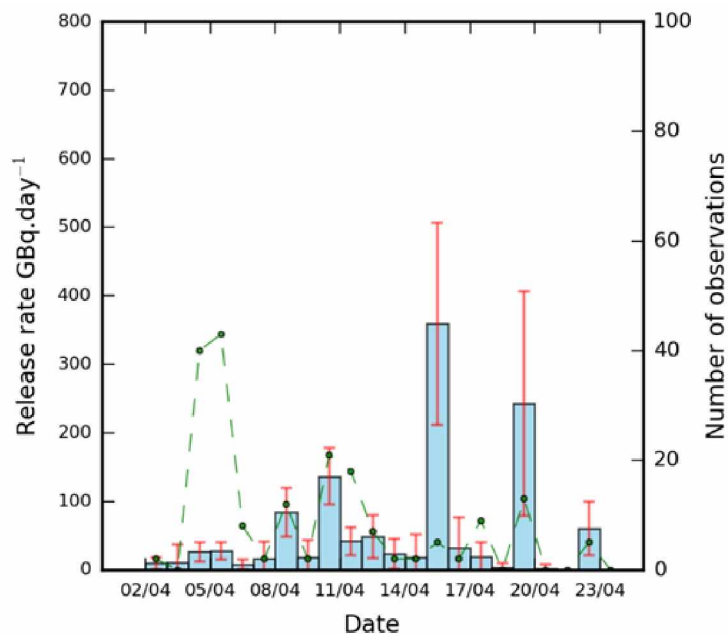
229 In France, the maximum weekly ^{137}Cs activity level reached $1.31 \pm 0.24 \mu\text{Bq}\cdot\text{m}^{-3}$ from April 6 to 14, 2020
230 and was observed in the southeastern corner. It confirms model forecasts indicating that the highest value
231 occurred in that region during this period. The weekly average ^{137}Cs value measured during the fire event
232 was thus 4 to 8 fold higher than the ^{137}Cs background level in SE of France. The IRSN estimated that the
233 average ^{137}Cs level added by fires in Ukraine during the presence of the air mass in France was at most 2
234 $\mu\text{Bq}\cdot\text{m}^{-3}$ which is of no health concern for the public. For that purpose, the average regional background
235 ^{137}Cs level (0.15 to $0.30 \mu\text{Bq}\cdot\text{m}^{-3}$) determined in a period ranging from March 15 to May 15 over the past 5
236 years was removed for the remaining sampling period. Finally, the amount of ^{137}Cs corresponding to the
237 presence of the smoke plume was divided by the air volume filtered during its estimated presence. The
238 concentration of airborne ^{137}Cs measured in France in April 2020 had not been observed since 2002 (from
239 the end of August to the end of September 2002) when airborne ^{137}Cs concentrations increased up to
240 $3.5 \mu\text{Bq}\cdot\text{m}^{-3}$. This increase also resulted from wildfires raging in the Chernobyl area when for short periods
241 the usual prevailing westerly wind was not in place. Winds were in fact easterly during Week 36 and Week
242 38, 2002, leading to twin spikes in the concentration of airborne ^{137}Cs in France, Germany, Czech Republic,
243 and Austria. Outside the Chernobyl area, the highest airborne ^{137}Cs activity level was measured in Vilnius,
244 Lithuania with up to $196 \mu\text{Bq}\cdot\text{m}^{-3}$ during Week 36, 2002.¹³ At that time, there were also a lot of fires in the
245 vicinity of Vilnius,⁴⁶ which were responsible for an increase in PM_{10} up to $370 \mu\text{g}\cdot\text{m}^{-3}$. Due to a higher
246 water-soluble ^{137}Cs percentage, Lujaniene et al. (2006) concluded that these particulate matters were
247 transported to Lithuania from forest fires occurring in Ukraine and Belarus.¹³ Rising ^{137}Cs activity
248 concentrations from smoke are due to both the enhancement of the airborne dust load, acting as ^{137}Cs carrier,
249 but also to the fact that smoke is significantly rich in ^{137}Cs .³¹

250 We took the opportunity of this event to check if other radionuclides emitted into the atmosphere by
251 wildfires might be used, in combination with ^{137}Cs , as a tool to attest the contribution of the wildfire plume
252 far from the Chernobyl area. Strontium-90, plutonium isotopes, and ^{241}Am might be candidates. However,
253 their tedious radiochemistry complicates their determination and their much lower expected airborne
254 concentrations as compared to ^{137}Cs usually requires to gather together several weekly filters to exceed the
255 detection limit in the composite sample. These RN are thus difficult to quantify above detection limits on a
256 weekly aerosol-sampling basis. Looking for a more convenient-to-measure radionuclide whose activity ratio
257 with ^{137}Cs might be relevant for wildfire plume detection at long distances, we also examined the airborne
258 ^{40}K concentrations (See SI).

259

260 **Source term assessment methodology**

261 The UHMI performed RN source terms assessment based on environmental parameters such as satellite
262 observations of burned areas, biomass density, and contamination density maps. Another way to assess
263 radionuclide amounts emitted from the burned areas is to apply inverse modeling techniques combining
264 atmospheric transport model and observed airborne concentrations. Such methodology was implemented
265 using the comprehensive airborne ^{137}Cs dataset acquired on the European scale (see Table S6, SI) to estimate
266 first the amounts of ^{137}Cs emitted into the atmosphere between April 2 and April 24, 2020. The method is
267 described in the SI. Twenty-two different daily releases were estimated by inverse modeling between April
268 2 and 24, 2020. Although satellite images after April 24 indicate a persistent residual fire, releases were
269 assumed insignificant after that date. In addition, the available measurements after April 24 are clearly not
270 sufficient for an inverse modeling estimation of the source term. Our inverse modelling is based on a
271 variational approach which consists in the minimization of a least-squares cost function assuming log-
272 normal observations errors and without considering any additional background term (see SI). Performing
273 Monte-Carlo simulations, 15,000 different source terms were computed in order to take into account
274 uncertainties resulting both from dispersion modeling, meteorological fields and representation errors of
275 observations. For instance, this analysis indicates that the estimated ^{137}Cs source term for the entire fire
276 period lies between 700 and 1,200 GBq. This range reflects the set of all the above mentioned uncertainties.
277 From April 2 to 15, our results indicate daily ^{137}Cs emissions ranging from 10 to 138 GBq (Figure 2). For
278 this period, the source term estimation proves to be fairly robust since the sensitivity to observation
279 perturbations is weak. The large number of observed values considered in the inverse modeling process
280 reasonably explains the standard deviation on daily release rates remaining low. From April 15, the
281 magnitude of the daily release rates varied significantly. The maximum daily release rate reached 362 GBq
282 on April 16 and 241 GBq on April 20 thus corresponding to the highest releases estimated during the entire
283 fire period. However, the standard deviations calculated for April 16 and 19 are large. This increases the
284 source term margin of error and leads to a higher level of uncertainty.



285
 286 Figure 2: April 2 to 24 ¹³⁷Cs average daily release rates reconstructed by Monte Carlo analysis using n=
 287 15,000 samples (blue rectangles) and the associated standard deviations (orange bars). The green dashed
 288 line represents the number of observations used for each daily release assessed by inverse modeling.

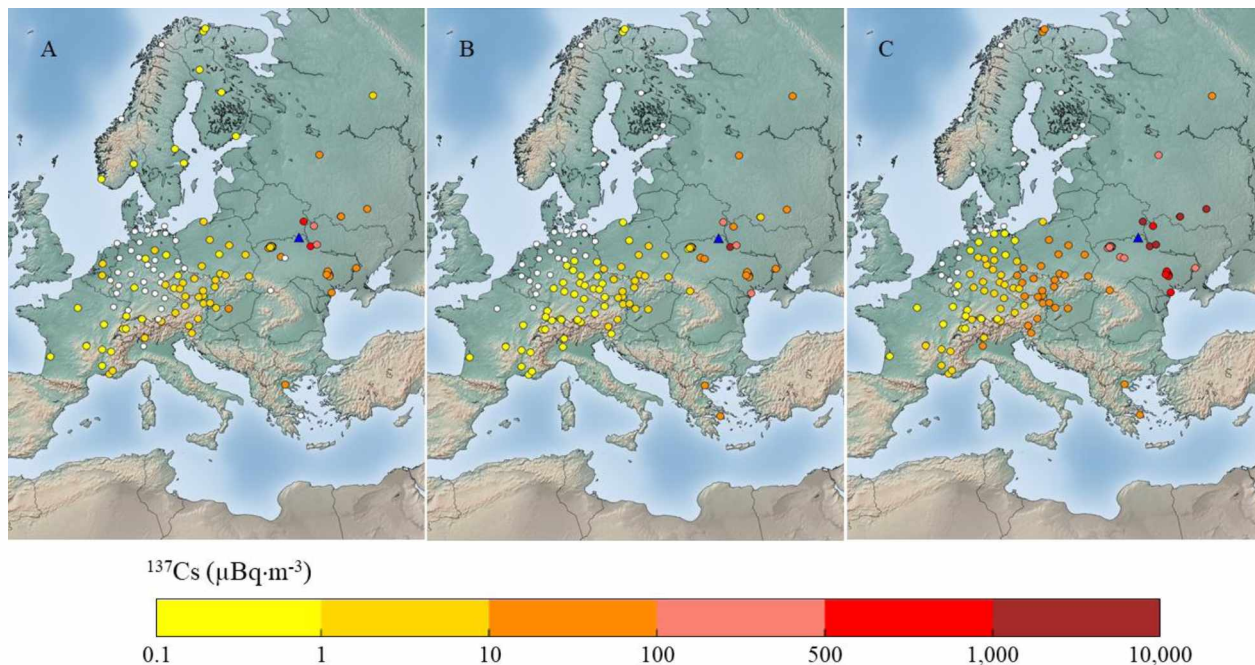
289

290 **Plume dispersion analysis**

291 The video of the plume dispersion simulation is available in the SI. An average source term was deduced
 292 from the Monte Carlo analysis as an input parameter. The smoke plume first went in the direction of the
 293 Russian Federation between April 2 and 3. From April 3 to 5, it moved to the south of Ukraine (including
 294 the Kiev region). From April 5 to 7, the plume continued to move towards both the west and south. It reached
 295 Romania, Hungary, the Czech Republic, eastern Poland, Austria and Slovenia during this period. The
 296 simulated hourly ¹³⁷Cs concentrations are about 10 - 50 μBq·m⁻³, sometimes higher in eastern Romania and
 297 much lower to the west. From April 7, according to the model, there were very low ¹³⁷Cs concentrations
 298 (just above 1 μBq·m⁻³) in southern Germany, France and Italy. These levels are close to the detection limits
 299 (DL). The model provides an explanation as to why the vast majority of sampling stations located in this
 300 geographical area did not report any concentration higher than DL. Furthermore, even in the case of a
 301 measurement > DL, as for instance in Austria and Poland, these measurements did not vary from the usual
 302 seasonal values. Modeling still tends to emphasize a contribution in ¹³⁷Cs concentrations from the fire,
 303 especially in the Czech Republic, Austria, Italy, Slovenia and France. Between April 8 and 10, a new plume
 304 reached the south of Ukraine again. The plume extended to Greece as of April 11. The hourly-simulated
 305 concentration reached up to 100 μBq·m⁻³ in the Thessaloniki area.

306 This estimate is fully consistent with measurements performed in Thessaloniki between April 11 and 13
307 with an average concentration of $25.5 \mu\text{Bq}\cdot\text{m}^{-3}$ and a residence time of $3.5 \pm 0.2 \text{ d}$.⁴⁷
308 The wind direction changed again between April 12 and 13. Consequently, the wind blew towards Russia.
309 This change in direction corresponded to the most significant release period when the hourly simulated
310 concentrations exceeded $100 \mu\text{Bq}\cdot\text{m}^{-3}$ at the IMS Russian station in Dubna. The plume then moved
311 northwest, to the northernmost part of Norway. The simulation shows hourly values up to $30 \mu\text{Bq}\cdot\text{m}^{-3}$ over
312 this area on April 14. The plume passed through this region relatively quickly, in about a few hours. This
313 explains why the weekly sampling carried out in Svanhovd showed little variation compared to weekly
314 averages with a concentration of only $0.5 \mu\text{Bq}\cdot\text{m}^{-3}$. This value is likely the result of fires being controlled.
315 During this period, very low weekly average ^{137}Cs concentrations were reported in Western Europe (about
316 $1 \mu\text{Bq}\cdot\text{m}^{-3}$). From April 15 to 19, the wind mainly blew east and southeast. Several slightly contaminated
317 air masses mainly affected the Kiev region and the more southern regions of Ukraine. On April 21, the
318 plume reached Greece again. The simulation consistently matched measurements carried out in Thessaloniki
319 ($9.6 \pm 0.8 \mu\text{Bq}\cdot\text{m}^{-3}$) on April 21 with an estimated residence time of $11 \pm 3 \text{ d}$.⁴⁷
320 55% of the simulated ^{137}Cs concentrations were within a factor of 2 compared to the observed concentrations
321 (see Table S5, SI). This score provides significant validation of the reconstructed source term (see SI).
322 Maximum simulated and observed ^{137}Cs concentrations are compared from April 2 to 24 (Figure 3). The
323 observed and simulated ^{137}Cs maximum concentrations (maps A and B) are very similar. The maximum
324 simulated concentrations in Ukraine, Belarus and the Russian Federation are the highest and are consistent
325 with the maximum concentration levels reported in these countries. Further west, the correlation between
326 simulated and observed concentrations is also satisfactory, although the model tends to underestimate the
327 maximum observed concentrations in Austria. In any case, the maximum concentrations measured in this
328 area are low and the usual ^{137}Cs background level would have to be rigorously taken into account, if known,
329 in order to make a proper comparison between observed concentrations and simulated concentrations added
330 by the plumes. As a result of the agreement between simulations and observations, the hourly maximum
331 simulated ^{137}Cs concentration was derived at each sampling location (Figure 3, map C). Due to the spatial
332 resolution of the long-range dispersion model, values obtained at less than 50 km from the CNPP were not
333 taken into account because of the significant associated uncertainties. The maximum hourly concentrations
334 simulated in Eastern Ukraine, the western part of the Russian Federation and southern Belarus were above
335 $1 \text{ mBq}\cdot\text{m}^{-3}$ (Figure 3, map C). Simulated concentrations then gradually decreased to the west. They were
336 above $10 \mu\text{Bq}\cdot\text{m}^{-3}$ over a central band stretching from northern Norway to southern Greece. Further west,
337 concentrations were even lower but still above $1 \mu\text{Bq}\cdot\text{m}^{-3}$ in southern France, Switzerland, western Austria
338 and Germany. This confirms that the ^{137}Cs concentrations measured in these countries were partly due to
339 the influence of the remote fire despite values being very close to observed seasonal measurements.

340 However, in Belgium and in the Netherlands, unusual ^{137}Cs concentrations (5.3 and 1.59 $\mu\text{Bq}\cdot\text{m}^{-3}$,
341 respectively) were locally reported, that both our dispersion simulation and that of SCK-CEN cannot
342 reproduce. It has been suggested that a local/regional simultaneous resuspension event might be the reason
343 of the discrepancies between modeling and observations.

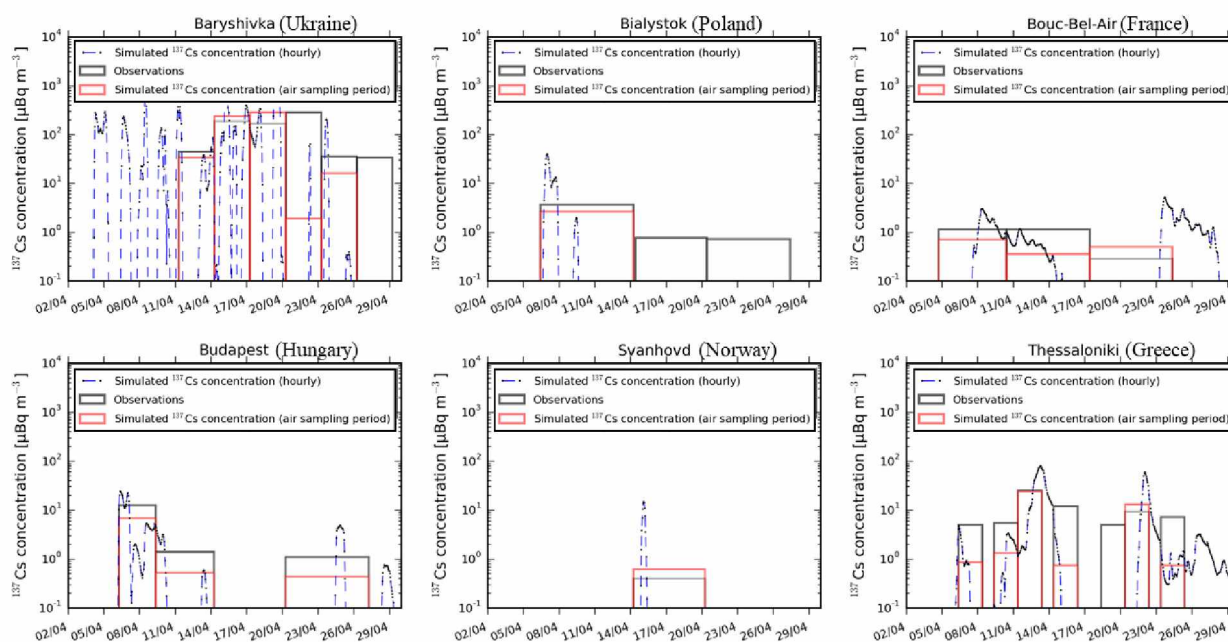


344
345 Figure 3: ^{137}Cs airborne concentration maps ($\mu\text{Bq}\cdot\text{m}^{-3}$) over the course of the April, 2020 wildfire event in
346 Ukraine. (A) Maximum observed concentrations; (B) Maximum simulated concentrations; (C) Maximum
347 values based on hourly simulated concentrations (i.e. maximum time-resolved peak concentrations). The
348 same color scale applies to all maps.

349
350 According to Figure 4, the plume passed through Ukraine several times. At the Baryshivka station,
351 hourly simulated concentrations exceeded 1 $\text{mBq}\cdot\text{m}^{-3}$ between April 17 and 20. In Greece, fire
352 plumes reached the Thessaloniki area (northern Greece) on three occasions. The most significant
353 episode around April 13 in this area was characterized by hourly simulated concentrations up to
354 100 $\mu\text{Bq}\cdot\text{m}^{-3}$. The average ^{137}Cs estimated concentration over the air sampling period (20 to 30
355 $\mu\text{Bq}\cdot\text{m}^{-3}$) remains consistent with measurement taken in Thessaloniki (25.5 $\mu\text{Bq}\cdot\text{m}^{-3}$). Further
356 south, in Athens, no observable ^{137}Cs activity concentration ($> 3 \mu\text{Bq}\cdot\text{m}^{-3}$) was determined on three
357 consecutive filters sampled from April 3 – 15. The geographical extent of the plume was very large
358 as it reached as far as the northernmost part of Norway for a few hours on April 15 with a peak

359 simulated concentration of about $20 \mu\text{Bq}\cdot\text{m}^{-3}$ in Svanhovd. However, as the plume passed very
 360 quickly the concentration evaluated between April 14 and 20 remained below $1 \mu\text{Bq}\cdot\text{m}^{-3}$, which is
 361 consistent with locally reported measurements. Further west, in Bialystok (Poland), Budapest
 362 (Hungary) and Bouc-Bel-Air (south of France), the simulation matched observation though the
 363 simulation underestimated values slightly. This discrepancy can be explained by the contribution
 364 of the usual ^{137}Cs background which represents a significant part of the total airborne concentration,
 365 especially when it is low, as is the case in France and to a lesser extent in Poland. According to the
 366 simulation, two plumes reached southeastern France between April 2 and April 24. The first plume,
 367 characterized by very low concentrations (estimated 2 to $3 \mu\text{Bq}\cdot\text{m}^{-3}$), reached this region between
 368 April 8 and 15. A second plume arrived in Bouc-Bel-Air between April 23 and 29, but its magnitude
 369 remains imprecise due to the higher uncertainty resulting from the source term reconstructed during
 370 this time lapse. Comparisons at other European locations are provided in the SI (see Figure S7, SI).
 371 Dates and times of maximum simulated ^{137}Cs concentrations are also tabulated in the SI.

372



373

374 Figure 4: Example of comparisons between simulated and observed airborne ^{137}Cs concentrations
 375 at several European locations. The grey line shows the observed concentrations for each sampling
 376 period and the red line the simulated concentrations. The blue dashed line represents the simulated
 377 hourly concentrations.

378

379 ⁹⁰Sr, ²³⁸Pu, ²³⁹⁺²⁴⁰Pu emissions

380 Because of the facility researchers have measuring ¹³⁷Cs at trace levels using γ -spectrometry, most
381 investigations and reported data during this event focused on airborne ¹³⁷Cs as a tracer of biomass burnings,
382 both on a nation-wide scale (i.e. in Ukraine) and on a continental scale. However, owing to their respective
383 dose coefficients, there is much concern about the emission by wildfires of radionuclides such as ⁹⁰Sr, Pu
384 isotopes, and ²⁴¹Am. Strontium-90 as well as ²³⁸Pu and ²³⁹⁺²⁴⁰Pu were measured only inside the CEZ but not
385 on a wider scale. This prevented the use of the inverse methodology described for ¹³⁷Cs to assess: 1) the
386 corresponding source terms 2) resulting airborne concentrations elsewhere in Ukraine and in the rest of
387 Europe and 3) internal exposure. In France, all the filters taken at sampling stations that were assumed to be
388 in the path of the fire plume according to the dispersion analysis, in addition to a slightly higher observed
389 ¹³⁷Cs concentration than normal, were gathered in a composite sample representing 365,775 m³. The
390 following analyses were performed on this composite sample: α -spectrometry (²³⁸Pu, ²³⁹⁺²⁴⁰Pu, ²⁴¹Am), ICP-
391 MS (²³⁹Pu and ²⁴⁰Pu separately), proportional counting (⁹⁰Sr). Results for ²³⁸Pu (0.12 ± 0.07 nBq·m⁻³) and
392 ²³⁹⁺²⁴⁰Pu (3.43 ± 1.09 nBq·m⁻³) were in the usual background ranges reported in France over the last decade
393 ($0.03 - 0.42$ nBq·m⁻³ for ²³⁸Pu and $0.10 - 2.85$ nBq·m⁻³ for ²³⁹⁺²⁴⁰Pu). Strontium-90 remained below a decision
394 threshold of 62 nBq·m⁻³. As previously mentioned (see section *Plume detection in Ukraine*), emitted ⁹⁰Sr
395 bound in general to the coarse aerosol fraction and is found to travel only short distances from a fire.
396 Conversely, Yoschenko et al. demonstrated that transuranic elements which are in general bound to the fine
397 aerosol fraction, are prone to travel much greater distances from the emission point.³² Because of a high
398 (60%) relative uncertainty associated to the ²³⁸Pu result, the ²³⁸Pu/²³⁹⁺²⁴⁰Pu activity ratio observed in France
399 was not appropriate to discriminate a possible Chernobyl signature. However, the ²⁴⁰Pu/²³⁹Pu mass ratio
400 (0.25 ± 0.07) was slightly higher than the average value of 0.176 ± 0.03 usually observed in France during
401 the last decade and which is typical of global fallout. Given the 0.41-0.42 typical signature of the Chernobyl
402 fallout, this intermediate value could correspond to the added contribution following the smoke plume
403 arrival in France in April.

404 To cope with the lack of large scale Sr and Pu results during this event we used the generally accepted
405 Chernobyl-ratios between the above-mentioned radionuclides and airborne ¹³⁷Cs, and assumed these ratios
406 to be representative of the emissions. Given the internuclide relationships derived from previous measured
407 concentrations in the CEZ⁴⁸ and taking into account the previously estimated ¹³⁷Cs source term range (700
408 – 1,200 GBq), we considered the uncertainty associated with the relationships established between ⁹⁰Sr and
409 ¹³⁷Cs on one hand and between ²³⁸, ²³⁹⁺²⁴⁰Pu and ¹³⁷Cs on the other hand (Table 1).

410

411 Table 1: Estimations of Chernobyl-labelled radionuclides emissions (in GBq) during the April 2020 wildfires in Ukraine. Values for ^{137}Cs , ^{90}Sr , ^{238}Pu and
 412 $^{239+240}\text{Pu}$ are derived from field measurements. Those for ^{239}Pu , ^{240}Pu , ^{241}Pu and ^{241}Am are deduced from typical activity or isotopic ratios characteristic
 413 of the Chernobyl accident. The grand total source term ($^{137}\text{Cs} + ^{90}\text{Sr} + ^{238}\text{Pu} + ^{239}\text{Pu} + ^{240}\text{Pu} + ^{241}\text{Pu} + ^{241}\text{Am}$) has been evaluated from values in bold characters.

Radionuclide		This study						Other studies				
		Relationships used	R ² coef.	Estimated emission range (GBq)	Rounded average (GBq)	Ratio to ^{137}Cs (%)	% of total ST (%)	Protsak et al. ²¹ (GBq)	Tabachnyi et al. ³⁰ (GBq)	Talerko et al. ⁴⁹ (GBq)	De Meutter et al. ⁵⁰ (GBq)	Evangelioiu et al. ³⁸ (GBq)
^{137}Cs	(M)			700 – 1,200	950	100	62.2	690	660 – 945	574	220 -1,810	341
^{90}Sr	(M)	$^{90}\text{Sr} = 0.3313 [^{137}\text{Cs}]^{1.061 \pm 0.030}$	0.8318	346 – 613	480	50.4	31.5	13.5	n.d.	n.d.	n.d.	51
^{238}Pu	(M)	$^{238}\text{Pu} = 0.0009 [^{137}\text{Cs}]^{1.0833}$	0.9296	1.1 – 1.9	1.5	0.16	0.1	n.d.	n.d.	n.d.	n.d.	2
$^{239+240}\text{Pu}$	(M)	$^{239+240}\text{Pu} = 0.0023 [^{137}\text{Cs}]^{1.0756}$	0.9389	2.6 – 4.7	3.7	0.39	0.2	n.d.	n.d.	n.d.	n.d.	0.099
$^{238}\text{Pu} + ^{239+240}\text{Pu}$	(M)	$^{238,239+240}\text{Pu} = 0.0032 [^{137}\text{Cs}]^{1.0771}$	0.9375	3.7 – 6.7	5.2	0.55	0.3	0.059	n.d.	n.d.	n.d.	2.1
^{239}Pu	(D)	$^{239}\text{Pu} / ^{239+240}\text{Pu} = 0.403 (*)$		1.1 – 1.9	1.5	0.16	0.1	n.d.	n.d.	n.d.	n.d.	0.033
^{240}Pu	(D)	$^{240}\text{Pu} / ^{239}\text{Pu} (\text{activity}) = 1.496 (**)$		1.6 – 2.9	2.2	0.23	0.1	n.d.	n.d.	n.d.	n.d.	0.066
^{241}Pu (2020)	(D)	$^{241}\text{Pu} / ^{239+240}\text{Pu} (\text{activity}) = 19.1$		50.5 – 90.1	70.3	7.4	4.6	n.d.	n.d.	n.d.	n.d.	
^{241}Pu (2020)	(D)	$^{241}\text{Pu} / ^{239}\text{Pu} (\text{activity}) = 39.75$		42.3 – 75.6	59.0	6.2	3.9	n.d.	n.d.	n.d.	n.d.	n.d.
^{241}Am (2020)	(D)	$^{241}\text{Am} / ^{241}\text{Pu} = 0.328$		13.9 – 29.6	21.7	2.3	1.4	n.d.	n.d.	n.d.	n.d.	0.504
$^{137}\text{Cs} + ^{90}\text{Sr} + \Sigma\text{Pu} + ^{241}\text{Am}$				1,114 – 1,939	1,530		100					

414 (M): measured, (D): deduced, ST: Source Term, n.d.: not determined

415 (*) Values taken from ref.⁴⁸ for the organic layer of the surface soil (litter and humus).

416 (**) derived from the low-uncertainty $^{240}\text{Pu} / ^{239}\text{Pu}$ (isotopic) ratio 0.408 ± 0.003 obtained by Muramatsu et al.⁴⁸ in the Chernobyl environment.

417

418 Our ^{137}Cs source term estimation is fully consistent with that proposed by Ukrainian researchers: 690 GBq
419 as of April 20 or 660 to 945 GBq until the end of the blaze event.^{21, 30} These estimates are based on a very
420 different method combining land cover and vegetation features, radionuclide distribution in the ecosystem,
421 biomass burning emission factors, and fire satellite detections. Evangeliou & Eckhardt indicated that their
422 model underestimated measurements by about 70%, which means that in their study the average modeled
423 concentration was almost half of the average measured concentration.³⁸ Based on observed airborne
424 concentrations, our estimated average ^{90}Sr emission (480 GBq) is much higher than those estimated by
425 Protsak et al. (13.5 GBq) and Evangeliou & Eckhardt (51 GBq). These two ^{90}Sr assessments combined
426 estimations of the residual ^{90}Sr biomass contamination, satellite detections and used a ^{90}Sr emission factor
427 of 0.2% (i.e. 25-fold lower than for ^{137}Cs , based on their research). Our ^{238}Pu estimate is also consistent with
428 that of Evangeliou & Eckhardt.³⁸ However, the $^{238}\text{Pu}/^{239+240}\text{Pu}$ activity ratio (~20) indicated by these
429 authors³⁸ represents a serious discrepancy and is inconsistent with the characteristic Chernobyl Pu isotopic
430 signature of 0.48 or with the value of 0.47 typical of the residual contamination observed in 2000 in
431 Ukraine.^{42, 44} In our study, the relationship obtained between ^{238}Pu and $^{239+240}\text{Pu}$ can be expressed by $^{238}\text{Pu} =$
432 $0.384[^{239+240}\text{Pu}] - 0.0436$ ($R^2 = 0.9939$). The slope of the $^{238}\text{Pu}/^{239+240}\text{Pu}$ adjustment (0.384) fits the one
433 characteristic of the Chernobyl accident (0.4 - 0.5).

434

435 ^{239}Pu and ^{240}Pu emissions

436 Distinct determinations of ^{239}Pu and ^{240}Pu were not reported. Both Pu isotopes behave similarly in the
437 environment and have a much longer half-life as compared with the period of time that went by since the
438 accident, thus we can neglect their differential decay. We can assume that the $^{240}\text{Pu}/^{239}\text{Pu}$ ratio at the
439 emission to be the same as in soil or in the biomass. Muramatsu et al.⁴⁸ indicated a relative consistency of
440 the mass (or atom) ratio (average 0.408 ± 0.003 , range 0.386 - 0.412) regardless of the $^{239+240}\text{Pu}$
441 concentrations range in surface soil samples (i.e. organic rich layers). In some moss and soil samples of
442 Chernobyl, Jakopic et al.⁵¹ reported mass ratios of 0.3624 ± 0.0011 and 0.4140 ± 0.0035 , respectively. In
443 forest soil, a mass ratio ranging from 0.186 to 0.348 was found.⁵² We retain an average $^{240}\text{Pu}/^{239}\text{Pu}$ mass
444 ratio of 0.41 which once expressed in $^{240}\text{Pu}/^{239}\text{Pu}$ activity ratio corresponds to a value of 1.50, close to the
445 characteristic activity ratio (1.40) that can be deduced from the Chernobyl releases (see Table S1, SI).
446 Plutonium-239 can also be expressed with reference to $^{239+240}\text{Pu}$ with a typical activity ratios ($^{239}\text{Pu}/^{239+240}\text{Pu}$)
447 of 0.403.⁴⁸ Based on our $^{239+240}\text{Pu}$ emission estimate (2.6 – 4.7 GBq) we derived a ^{239}Pu emission between
448 1.1 and 1.9 GBq and a ^{240}Pu emission between 1.6 and 2.9 GBq.

449

450 ^{241}Pu and ^{241}Am emissions

451 Unfortunately, for the sake of study, no ^{241}Pu or ^{241}Am determination was reported for that event. Plutonium-
452 ^{241}Pu releases during the Chernobyl accident (~ 6 PBq) was the largest contributor to the total plutonium
453 released amount (see Table S1, S1). Despite its rather short half-life ($T_{1/2} = 14.4$ yr.), ^{241}Pu still denotes a
454 significant reservoir of environmental radioactivity. However, as a pure β emitter (maximum energy of only
455 20.8 keV) ^{241}Pu represents a lesser radiological risk compared with other α -emitting plutonium isotopes
456 (except via its decay product ^{241}Am). Since the Chernobyl accident, only 19.1% of the ^{241}Pu amount released
457 in 1986 is still present in the environment. It is possible to assess the ^{241}Pu emission by the April 2020
458 wildfires using the original $^{241}\text{Pu}/^{239+240}\text{Pu}$ activity ratio and applying a simple ^{241}Pu decay. This ratio was
459 estimated for May, 1986 in a range between 70 and 100.^{43, 53-57} or even in a range of 82 to 120 in upper parts
460 of lichens, 98 in air filter (May 1, 1986), 95 in grass (May 1, 1986).⁵⁶ Considering a global average ratio of
461 100 at the time of the accident and neglecting ^{239}Pu and ^{240}Pu decays as of April 2020, the $^{241}\text{Pu}/^{239+240}\text{Pu}$
462 activity ratio would have been about 19.1 during the wildfire event. Given the previously estimated $^{239+240}\text{Pu}$
463 emission (2.6 – 4.7 GBq) results in a ^{241}Pu emission between 50.5 and 90.1 GBq. Another estimation of the
464 ^{241}Pu emission can be performed using the initial $^{241}\text{Pu}/^{239}\text{Pu}$ mass ratio of 0.123 ± 0.007 (ref.⁵⁵) for May
465 1986 and confirmed by the value of 0.0384 ± 0.0022 determined for 2009.⁵¹ Once expressed in activity ratio
466 and ^{241}Pu -decay corrected to date, the $^{241}\text{Pu}/^{239}\text{Pu}$ activity ratio is 39.75. Considering the above estimated
467 ^{239}Pu emission range (1.1 – 1.9 GBq) leads to a ^{241}Pu emission ranging 42.3 – 75.6 GBq, consistent with the
468 above-mentioned estimation based on the $^{241}\text{Pu}/^{239+240}\text{Pu}$ ratio (50.5 – 90.1 GBq).

469 Most radiological concern comes from ^{241}Am . This nuclide results from ^{241}Pu decay and is characterized by
470 a much longer half-life ($T_{1/2} = 432.7$ yr.), a much higher radiotoxicity (as an α - γ emitter), and a higher
471 environmental mobility than its parent.⁵³ As a result, the in-growth of ^{241}Am from ^{241}Pu decay exhibits an
472 increasing radiation risk with time. By 2058, the ^{241}Am activity will exceed that of plutonium isotopes by
473 about a factor of two.⁵⁸ In addition, its inhalation effective dose coefficient is about 245 fold higher than for
474 ^{241}Pu . A deeper insight into the differential soil-to-plant transfer of both Pu and Am is necessary to assess
475 the ^{241}Am emission from that of ^{241}Pu . For both radionuclides, the downward migration in soil is expected
476 in the same range ($0.1 - 0.5$ cm-yr⁻¹). However, a 1.5 fold higher migration velocity has been reported for
477 ^{241}Am as compared with Pu in the Chernobyl-contaminated environment of Belarus characterized by sandy
478 soil of various types (soddy podzolic sand, loamy sand and peat bog).⁵⁸ Despite a high variability induced
479 by both plant species and soil structure and composition, both concentration factors (Cf_{Am} and Cf_{Pu}) between
480 soil and plant (root uptake path) remain much lower (2 to 3 order of magnitude less) compared to ^{137}Cs and
481 even more so to ^{90}Sr .^{54, 58, 59} As a rule of thumb, the ^{241}Am soil-to-plant concentration factor (Cf_{Am}) exceeds
482 that for Pu.^{58, 60} Sokolik et al.⁵⁸ proposed an average Cf_{Am} to Cf_{Pu} ratio of 2.2 (1 – 6 range) for meadow
483 grasses. Other determinations indicating a higher Cf_{Am} to Cf_{Pu} ratio were reported: about a factor of 2 in
484 crops⁶¹ and 2.3 (1.6 - 3.3 range) in bilberry and lingonberry plants.⁵⁹ Concentration factors from forest litter

485 to spruce and pine needles, to pine root and stem, to spruce bark, to fern, alder and heather have been
486 summarized in Mietelski et al.⁵⁴ with a similar average of 2.6 (0.3 - 5.7 range). Based on the above-mentioned
487 values and as a conservative approach, we considered hereafter a differential soil-to-plant transfer between
488 ²⁴¹Am and ²⁴¹Pu (Cf_{Am}/Cf_{Pu}) of 2.4. In the same period of time (34 yr.) since the Chernobyl accident, the
489 ingrown ²⁴¹Am represents 2.6% of the ²⁴¹Pu initially released. We can neglect the ingrowth of ²⁴¹Am stored
490 in the burnable biomass because 90% of the Pu is stored in the litter with a degradation rate of about a few
491 years.³² As of April 2020 the theoretical activity ratio ²⁴¹Am/²⁴¹Pu from Chernobyl was thus about 13%.
492 Multiplying this ratio by the above-mentioned Cf_{Am}/Cf_{Pu} ratio of 2.4 leads to a ratio of 0.328 between the
493 amounts of ²⁴¹Am and remaining ²⁴¹Pu emitted into the atmosphere in April 2020. To cope with the lack of
494 experimental determination the same biomass burning emission factor (i.e. 1%) can safely be considered
495 for both RN since Pu and Am have a much higher boiling point as compared with the maximum expected
496 fire temperature. In such a case, their emission during wildfires is assumed to be mainly limited through the
497 uplift of ashes and not through the gas phase.^{5, 62} The higher ²⁴¹Am release potential thus likely arises from
498 its higher upstream soil-to-plant transfer. The slightly higher ²⁴¹Am release potential than for Pu is validated
499 by the experimental determination of the resuspension factor by wildfires (K) (see Tables S2 and S3, SI).⁶²
500 ⁶³ In short, given the overall range estimated for the ²⁴¹Pu emission (42.3 – 90.1 GBq) results in an ²⁴¹Am
501 emission estimation between 13.9 GBq (42.3 GBq x 0.328) and 29.6 GBq (90.1 GBq x 0.328).
502 The particular case of storage facility risks in the vicinity of the CNPP are detailed in the information notes
503 published by the IRSN.²⁵⁻²⁸ The Ukrainian authorities indicated that the spent fuel storage facility N1 (which
504 contains spent fuel from the Chernobyl NPP decommissioned in 2000) was located in the immediate area
505 of the NPP, thus safe from the fires. The spent fuel storage facility N2 located in the CEZ contains empty
506 tanks made of huge reinforced concrete structures surrounded by a fence. The authorities also said that the
507 Pidlisne storage facility, made of fireproof reinforced concrete structures and used to store nuclear waste,
508 was also located in a place at low risk to fires. As a precaution, the forest was cut down around the storage
509 facility to avoid the threat of fire, and the distance from green spaces was more than 100 meters.⁶⁴ In addition
510 to waste managed in the industrial zone around the sarcophagus and engineered disposal sites, non-
511 engineered near-surface trench dumps were used as waste repositories. In the early 2000's, ²⁴¹Pu was
512 responsible for approximately 20% of the overall activity, while ²⁴¹Am and ²³⁸Pu were responsible for 45%
513 and 15% of the total α -activity, respectively.⁶⁵ Considering the numerous waste disposal sites that contain
514 large amounts of radionuclides and that are in the immediate proximity to the CNPP, it is likely that their
515 radionuclide content was spared from fire as previously mentioned.⁶⁶ Indeed, their soil cover naturally
516 protects them. However, vegetation can grow in this soil, uptake radionuclides, and as a result, become
517 highly contaminated.⁶⁷ After the trenches were covered with soil, some of them were also planted with small
518 pine trees.⁶⁵ During the course of the trees' growth, partial uptake of the radionuclides buried in the trenches

519 occurs. These radionuclides are then distributed between the trees and the topsoil through litterfall. Waste
520 trenches are also periodically flooded by groundwater. As a result of a solution pH in the 4.8 – 5.1 range,
521 radionuclide dissolution of fuel particles and migration of the corresponding radionuclides can be more
522 effective in their proximity.⁶⁸ Thiry et al.⁶⁷ estimated that the maximum ⁹⁰Sr transfer will be reached 40
523 years after planting with 7% of the total ⁹⁰Sr content in the trench being transferred to the trees, and 12% to
524 the forest litter. According to the transfer calculation conducted by Thiry et al.⁶⁷ on waste buried (trenches),
525 the transfer of ⁹⁰Sr from soil to tree and litter has been estimated to be at most 7% and 12%, respectively
526 thus 19% for the burnable biomass. The ⁹⁰Sr transfer is thus 216 fold more efficient than that of ¹³⁷Cs,⁶⁷
527 resulting in a maximum ¹³⁷Cs transfer of only 0.09%. Recent work by Kashparov et al. confirms that the
528 activity of the mobile form of ⁹⁰Sr in the trench has presently reached its maximum value.⁶⁹ This results
529 from the decrease of the amount of remaining nuclear fuel particles not yet dissolved in topsoil and the
530 reduction of the ⁹⁰Sr soil-to-plant transfer due to its radioactive decay. Regarding Pu, it can be emphasized
531 that, unlike ¹³⁷Cs and ⁹⁰Sr, the transfer of plutonium to plants is extremely low; this element is therefore
532 present at only trace amounts in forest organic matter and remains fixed in the mineral soil fraction
533 contaminated in 1986. Yoschenko et al. estimated that its transfer to trees plus litter was 3.5 fold lower than
534 for ¹³⁷Cs.³² Using this ratio we can estimate a Pu concentration factor from soil to plant + litter burnable
535 biomass (Cf_{Pu}) of 0.026%. Taken this factor and considering the previously mentioned ratio Cf_{Am} / Cf_{Pu} of
536 2.4 results in a transfer factor for ²⁴¹Am (Cf_{Am}) of 0.0624%. In short, considering the biomass emission
537 factor of 4% (for ¹³⁷Cs and ⁹⁰Sr) and 1% (for Pu isotopes and ²⁴¹Am), the proportion of radionuclides emitted
538 into the atmosphere by the wildfires as compared to their trench content can be estimated at 0.036%, 7.6%,
539 0.0026% for ¹³⁷Cs, ⁹⁰Sr and Pu isotopes, respectively. The volume of waste in the replanted trenches is not
540 precisely known. The trenches are scattered over a total area of 450 ha in the CEZ (around 10⁶ m³).⁶⁵ A
541 more refined estimate of the potential radionuclide emissions could be performed based on the buried waste
542 amount and existing biomass on their surface. However, such specific estimates require further investigation
543 which is beyond the scope of this study.

544 **Dose assessment**

545 A dose assessment was performed on two categories of people: firefighters who took part in firefighting in
546 the CEZ and inhabitants of Kiev at about 100 km from the CEZ. Firefighters have already been identified
547 at risk in the event of a forest/bush fire over the dumps (storage trenches), as their occupational dose may
548 exceed the constraint of 0.3 mSv·yr⁻¹.⁶⁵ Their inhalation dose assessment was performed taking deliberately
549 a conservative approach with the followings assumptions: 1) the firefighters had no respiratory protection
550 (as part of Personal Protective Equipment, PPE) such as a self-contained breathing apparatus (SCBA) or a
551 facemask, 2) all aerosol sizes resulting from wildfires were belonging to the respirable fraction (<10 μm),

3) a total working time in the exclusion zone of a hundred hours for each of them (10 days with 10 working hours per day), 4) a breathing rate of $3 \text{ m}^3 \cdot \text{h}^{-1}$ corresponding to a very heavy exercise.⁷⁰ The airborne concentrations considered were based on field measurements where ^{137}Cs , ^{90}Sr , ^{238}Pu and $^{239+240}\text{Pu}$ were simultaneously measured (see Table S7, SI). Detailed estimations for ^{239}Pu , ^{240}Pu , ^{241}Pu and ^{241}Am (both not measured) were derived from measured ^{137}Cs concentrations and Pu isotopic ratio according to the relationships mentioned in Table 1. Two possibilities were considered for the measured values: maximum observed or average values. The first assumption, leading to airborne concentrations of $1 \text{ Bq} \cdot \text{m}^{-3}$ (rounded values) for both ^{137}Cs and ^{90}Sr , and $1 \text{ mBq} \cdot \text{m}^{-3}$ for ^{238}Pu , is very pessimistic since the highest measured concentrations at similar orders of magnitude were only reported during short periods of time (i.e. peak values over half an hour). Thus the consideration of such constant concentrations over a hundred-hour exposure is likely excessive and must be considered as an upper limit that could not be exceeded. This led to the following calculated airborne concentrations: $1 \text{ mBq} \cdot \text{m}^{-3}$ for ^{239}Pu , $1.5 \text{ mBq} \cdot \text{m}^{-3}$ for ^{240}Pu , $44 \text{ mBq} \cdot \text{m}^{-3}$ for ^{241}Pu and $12 \text{ mBq} \cdot \text{m}^{-3}$ for ^{241}Am . Given the above-mentioned considerations and the effective dose coefficients for workers (Table 2), the corresponding committed effective dose over an integration time of 50 years by inhalation of radioactive smoke at such RN concentrations would have reached 170 microSievert (μSv) in total of which 80% comes from ^{241}Am (Table 3). A much more likely dose assessment even if may be an underestimation can be established based on spatially averaged concentrations (Table 3). In this case, the resulting dose induced by inhalation of all artificial RN considered in this study over a period of 100 hours would be $1.3 \mu\text{Sv}$. These estimated doses are much lower than the internationally accepted maximum dose for the public from external sources ($1 \text{ mSv} \cdot \text{yr}^{-1}$).

Table 2: Effective dose coefficients ($\text{Sv} \cdot \text{Bq}^{-1}$) of RN of interest for the general public (adult) and for workers during wildfires.⁷¹

Radionuclide →	^{137}Cs	^{90}Sr	^{238}Pu , ^{239}Pu , ^{240}Pu	^{241}Pu	^{241}Am
Absorption type →	F	M	S	S	M
Dose coefficient (Sv Bq^{-1}) <i>Adult of the Public (*)</i>	$4.6 \cdot 10^{-9}$	$3.6 \cdot 10^{-8}$	$1.6 \cdot 10^{-5}$	$1.7 \cdot 10^{-7}$	$4.2 \cdot 10^{-5}$
Dose coefficient (Sv Bq^{-1}) <i>Workers (*)</i>	$4.8 \cdot 10^{-9}$	$3.6 \cdot 10^{-8}$	$1.5 \cdot 10^{-5}$	$1.6 \cdot 10^{-7}$	$3.9 \cdot 10^{-5}$

(*) aerosol diameter of $1 \mu\text{m}$.

Notes: Absorption types: F = Fast, M = Moderate, S = Slow. For ^{90}Sr , the type M corresponding to fuel fragments or when unspecified forms is recommended for the general public⁷² and for workers⁷³ even if there is no recommendation in⁷¹. For Pu isotopes a S-type solubility has been considered as a result of the Pu oxide forms released during the Chernobyl accident.

Despite rather high airborne ^{137}Cs concentrations measured near fire lines, the low ^{137}Cs dose coefficient, as compared with that of ^{90}Sr or Pu isotopes, minimizes its dose impact (only 1% of the total inhalation dose, Table 3). It is important to point out that the ^{137}Cs dose coefficient is 10 fold less significant than that of ^{90}Sr

584 (Table 2). Since airborne ^{90}Sr concentrations were only 0.8 fold lower than those of ^{137}Cs on average, ^{90}Sr
585 resulted in a greater average dose impact. As α -emitters, ^{238}Pu , ^{239}Pu and ^{240}Pu do not cause any significant
586 external exposure. However, owing to their high radiotoxicity, the contribution of transuranic elements by
587 inhalation to the exposure of firefighters is not something to ignore. Airborne Pu concentrations in the
588 proximity of fire lines were about 250 fold lower than ^{137}Cs concentrations on average. But the Pu effective
589 dose coefficients are about 3,500 fold higher than that of ^{137}Cs . These significant differences in dose
590 coefficients make $^{238,239,240}\text{Pu}$ isotopes definitively more significant dose contributors. This is almost the
591 same for ^{241}Am which emits mostly high-energy α -particles in addition to low-energy γ -rays ($E = 60$ keV,
592 13%). Eventually, the highest inhalation dose coefficient among the studied RN belongs to ^{241}Am which has
593 a dose coefficient of about 250 fold higher than that of ^{241}Pu . In any case, the estimated effective dose for
594 firefighters ($0.013 \mu\text{Sv}\cdot\text{h}^{-1}$) as a result of inhalation of those radionuclides remained lower than or similar to
595 the external exposure to radiation from the highly contaminated environment of the CEZ which is most
596 often between 0.1 and $1 \mu\text{Sv}\cdot\text{h}^{-1}$, and with maximum values about $10 \mu\text{Sv}\cdot\text{h}^{-1}$.^{6, 32} However, they may have
597 been significantly reduced (1 to 2 orders of magnitude) if protective equipment has been actually used.⁶

598
599 Table 3: Estimated effective doses (in μSv) by inhalation of artificial RN at a breathing rate of $3 \text{ m}^3\cdot\text{h}^{-1}$ and
600 during 100 hours, for firefighters in the CEZ during the April 2020 wildfires, for two scenarios:
601 (A) observed peak concentrations, (B) spatially averaged concentrations.

Scenario	Radionuclide	^{137}Cs	^{90}Sr	^{238}Pu	^{239}Pu	^{240}Pu	^{241}Pu	^{241}Am	Total
A	Maximum airborne concentration ($\text{mBq}\cdot\text{m}^{-3}$)	1000	1000	1	1	1.5	44	12	
	Bq inhaled after 100 h	300	300	0.3	0.3	0.4	13.2	3.6	
	Dose (μSv)	1.44	10.8	4.5	4.2	6.3	2.1	141	170
B	Average airborne concentration ($\text{mBq}\cdot\text{m}^{-3}$)	10	10	0.01	0.007	0.01	0.3	0.09	
	Bq inhaled after 100 h	3	3	0.003	0.002	0.003	0.09	0.027	
	Dose (μSv)	0.014	0.108	0.045	0.029	0.042	0.014	1.05	1.3
	Contribution to the total inhalation dose	1.1%	8.3%	3.5%	2.2%	3.2%	1.1%	80.6%	8,9%

602
603 The inhalation dose rate ($0.013 \mu\text{Sv}\cdot\text{h}^{-1}$) would have also remained about 8 fold lower than the average
604 ambient dose rate of $0.1 \mu\text{Sv}\cdot\text{h}^{-1}$ from the natural background.⁶ When considering maximum airborne
605 concentrations, the dose rate estimation ($1.7 \mu\text{Sv}\cdot\text{h}^{-1}$) by inhalation of artificial RN for firefighters is similar

606 to the order of magnitude of the external exposure dose rate from the highly contaminated environment (1
607 – 10 $\mu\text{Sv}\cdot\text{h}^{-1}$). It would have been 10 to 20 fold higher than the external ambient dose rate from natural
608 background radiation of 0.1 $\mu\text{Sv}\cdot\text{h}^{-1}$ (range 0.07 - 0.23 $\mu\text{Sv}\cdot\text{h}^{-1}$) and the internal dose of 0.18 $\mu\text{Sv}\cdot\text{h}^{-1}$ (range
609 0.05 - 1.3 $\mu\text{Sv}\cdot\text{h}^{-1}$), respectively.^{6, 63} Our estimates are consistent with those from previous studies,^{6, 62, 63}
610 which also indicate the predominant contribution of transuranic elements in the internal inhalation
611 exposure.⁶ These studies also point out that the dose received by firefighters because of smoke inhalation
612 (internal dose) was only about 1% of the dose induced by ground shine and the effective external dose would
613 have exceeded the expected internal dose for firefighters even without protective equipment.⁶ The dose of
614 external radiation from the smoke (cloud shine) in case of fire was not taken into account as it is negligible
615 (10^4 - 10^5 fold lower) as compared to the external dose (ground shine) from the contaminated environment.³²

616 Chernobyl-labeled radionuclides aside, naturally occurring radionuclides with a high dose coefficient and
617 that are prone to emission during a wildfire have to be considered. This is typically the case for, among
618 others, ^{210}Po ($T_{1/2} = 138$ d.) as a progeny of the relatively long-lived ^{210}Pb ($T_{1/2} = 22$ yr.) and which
619 accumulates in the biomass through foliar uptake. Polonium-210 has an effective dose coefficient of 3.3
620 10^{-6} Sv/Bq and 3.0 10^{-6} Sv/Bq for an adult of the public and for a worker, respectively, and given a type M
621 solubility corresponding to chloride, hydroxide, volatilized Po and all unspecified Po forms. Polonium is
622 among the radioactive elements with a low fusion point (about 254 °C for elemental Po under 1 atm). The
623 volatilization points of common polonium compounds are about 390 °C thus much lower as compared to
624 mean wildfire temperatures (> 500 °C with maximum of 1,000 –1,200 °C).⁵ As a result, ^{210}Po is easily
625 emitted during a fire. Carvalho et al. suggested that, as a result of combustion, a percentage of the ^{210}Po
626 initially in the biomass becomes concentrated in flying ash particles which corresponds to the refractory
627 remaining fraction after organic and water losses, while another percentage of the ^{210}Po forms gaseous ions
628 after volatilization which are likely to be captured by electrostatic forces onto smaller aerosol particles (<
629 0.5 μm), due to their higher surface/mass (or volume) ratio.⁵ Because of its high dose coefficient these
630 processes are a further reason to take ^{210}Po into account when estimating internal exposure during a wildfire.
631 Carvalho et al. measured a maximum airborne ^{210}Po concentration of 70 $\text{mBq}\cdot\text{m}^{-3}$ in the proximity of a fire
632 line in Portugal in the summer 2012.⁵ This concentration is as much as 1,000 fold higher as compared with
633 the airborne ^{210}Po background level of about a dozen $\mu\text{Bq}\cdot\text{m}^{-3}$ in the Northern hemisphere.⁷⁴ Since ^{210}Po was
634 not measured in April 2020, it is difficult to assert that such concentration would have been reached in the
635 CEZ even though wildfire conditions can be assumed to be similar. In order to adapt to the absence of ^{210}Po
636 measurement we propose to use a wider range of possible airborne ^{210}Po concentrations encompassing the
637 concentration found in Portugal, i.e. 1, 10 and 100 $\text{mBq}\cdot\text{m}^{-3}$, in order to provide the order of magnitude of
638 the inhalation dose assessment. We can estimate a maximum breathing rate at 3 $\text{m}^3\cdot\text{h}^{-1}$ for a firefighter

639 working 10 hours a day (as established by Kashparov et al., 2015) during 10 days.⁶ Based on a ²¹⁰Po
640 concentration of 10 mBq·m⁻³, the inhalation dose would increase by 9 μSv. This would represent 5% of the
641 inhalation dose from radionuclides originating from Chernobyl (¹³⁷Cs + ⁹⁰Sr + ΣPu + Am) when considering
642 maximum airborne concentrations. When considering average airborne concentrations this would result in
643 a 7 fold higher dose.

644 With the exception of the area in the immediate proximity to the fire, concentrations rapidly decreased and
645 did not present any concern for public health. At greater distances from the blaze, as in Kiev, the airborne
646 ¹³⁷Cs measured concentrations, or calculated concentrations for the other RN, remained between 1,000 and
647 10,000 fold lower on average than those in the CEZ and did not present any risk for the population, even
648 when considering ingestion of foodstuffs subject to radionuclide deposition. To compute airborne RN
649 concentrations for an inhabitant of Kiev, we used the previously calculated RN source terms (Table 1) as an
650 input parameter in the Eulerian Idx dispersion / deposition model developed by the IRSN (see *Source term*
651 *assessment methodology*). Subsequent RN deposition was computed assuming a dry deposition velocity of
652 0.2 cm·s⁻¹. Based on actual meteorological data, the effective dose induced both by inhalation (respiratory
653 rate of 22.18 m³·d⁻¹) and ingestion of foodstuffs following RN deposition was determined to be 150 nSv for
654 an adult (100 nSv for inhalation from April 1 to 22, 2020 and 50 nSv for ingestion over a period of 1 year
655 after deposition). The detailed inhalation dose per radionuclide is as follows: ¹³⁷Cs 0.1 nSv, ⁹⁰Sr 1 nSv, ²³⁸Pu
656 5 nSv, ²³⁹Pu 5 nSv, ²⁴⁰Pu 10 nSv, ²⁴¹Pu 5 nSv (ΣPu 25 nSv) and ²⁴¹Am 75 nSv. For the ingestion dose
657 calculation, the main agricultural products that were considered include vegetables in season (April), dairy
658 products and meat. The daily consumption of 500 g of leafy vegetables is considered as the most penalizing
659 scenario. As confirmed by Talerko et al.,⁴⁹ the dose induced by exposure to the cloud shine (immersion)
660 was negligible as compared with internal exposure. The total exposure was also negligible compared to the
661 annual public exposure limit of 1 mSv according to Ukrainian Radiation Safety Standards for the general
662 public as an added effective dose⁴⁵ or when compared to the average annual global exposure of 2.4 mSv
663 induced by natural background radiation.²⁹

664 Elsewhere in Europe, doses were even lower as airborne concentrations were much lower. At some distant
665 locations the contribution of the fire plume to the ¹³⁷Cs airborne concentration was estimated to be between
666 2 and 8-fold at most the usual ¹³⁷Cs trace-level concentration. Assuming consistent soil contamination as a
667 routine source of ¹³⁷Cs background emission (through soil particle resuspension) the use of the airborne
668 ¹³⁷Cs/⁴⁰K ratio has also proven to be helpful in the determination of fire plume contribution. However, the
669 proper use of this tool requires the knowledge of a local baseline value to distinguish any additional remote
670 ¹³⁷Cs input.

671 In anticipation of future wildfires in the Chernobyl area, the detailed study of the re-emission into the
672 atmosphere of Pu isotopes released during the Chernobyl accident or arising as their decay products (²⁴¹Am,

673 ^{237}Np), in addition to ^{90}Sr , ^{137}Cs , $^{243,244}\text{Cm}$ and naturally occurring radionuclides such as ^{210}Po during
674 wildfires is recommended for a more comprehensive estimate of the internal exposure by inhalation for
675 firefighters and for the population. It is also essential to point out that our knowledge of respective amounts
676 of radionuclides emitted both in gaseous phase according to their volatilization point and as aerosol particles
677 (flying ashes) is insufficient and requires further study. In the future, if forests are not thinned, exposure
678 risks from forest fire emissions are expected to increase due to the accumulation of debris, litter and standing
679 dead trees and because of early and lengthy droughts in the framework of climate change.

680 Lengthy wildfire outbreaks are a challenge for inverse modeling computation when they both vary in
681 location and magnitude. Such outbreaks are also an opportunity to strengthen international collaboration
682 between radioprotection organizations and demonstrate the benefits of rapid information sharing, which is
683 the main goal of the informal Ring of Five (Ro5) European monitoring network.

684
685 **Corresponding Author:** Olivier Masson, Email: olivier.masson@irsn.fr, ORCID:
686 <https://orcid.org/0000-0001-6209-6114>

687
688
689 **Author Contributions:** The manuscript was written through contributions of all authors. All authors have
690 given approval to the final version of the manuscript.

691 692 693 **Acknowledgments**

694 Authors are grateful to the following Ukrainian organizations for sharing their data and regular information
695 on the fire situation: the State Scientific and Technical Center for Nuclear and Radiation Safety (SSTC), the
696 Ukrainian Hydrometeorological Institute (UHMI), the State Specialized Enterprise Ecocentre (SSE), the
697 Central Geophysical Laboratory (CGO) in Kiev, the Rivne NPP. Authors address special thanks to
698 Intelligence System GEO (ISGEO, <http://www.isgeo.com.ua/> for the provision of the ^{137}Cs contamination
699 maps. We wish also to acknowledge the NASA for fire detections through the Fire Information for Resource
700 Management System Fire Information for Resource Management System (FIRMS) and the European Space
701 Agency (ESA) for the provision of Copernicus Sentinel-2 satellite images. We also thank all the Ro5
702 members involved during this event for the effort spent to insure airborne radioactivity monitoring through
703 aerosol sampling despite social confinement during the COVID-19 pandemic, and for stimulating
704 discussions. Special thanks to Paul Kloppenberg for English corrections. This paper is dedicated to the fire
705 brigades involved during this event.

706 707 **Supporting information**

708 The Supporting information contains the complete airborne radionuclide concentration dataset,
709 satellite images of fires spots and a video of the smoke plume dispersion over Europe. It also
710 contains 1) a review of historic wildfires in contaminated ecosystems, 2) knowledge about
711 radionuclide emission by fires in forested and non-forested lands, 3) information about long-lasting
712 persistence of airborne ^{137}Cs at trace-levels in Europe, 4) geographic analysis and timeline of the
713 April 2020 wildfire event in Ukraine, 5) information about the poor air quality observed in Kiev on
714 April 16, 2020, 6) radionuclide apportionment in the terrestrial ecosystem, 7) information about
715 data collection 8) information about the use of airborne ^{40}K and $^{137}\text{Cs}/^{40}\text{K}$ ratio for the identification
716 of a fire plume contribution, and 9) information about the methodology used for the source term
717 assessment.

718

719 **Competing interests**

720 The authors declare that they have no conflicts of interest.

721

722 **References**

723

- 724 1. Wotawa, G.; De Geer, L. E.; Becker, A.; D'Amours, R.; Jean, M.; Servranckx, R.; Ungar, K.,
725 Inter- and intra-continental transport of radioactive cesium released by boreal forest fires.
726 *Geophys. Res. Lett.* **2006**, *33*, (12).
- 727 2. Budyka, A. K.; Ogorodnikov, B. I., Radioactive aerosols formed owing to fires in regions
728 contaminated by products of Chernobyl accident. *Radiatsionnaya Biologiya. Radioekologiya*
729 **1995**, *35*, (1), 102-112.
- 730 3. Paliouris, G.; Taylor, H. W.; Wein, R. W.; Svoboda, J.; Mierzynski, B., Fire as an agent in
731 redistributing fallout ^{137}Cs in the Canadian boreal forest. *Sci. Total Environ.* **1995**, *160-161*,
732 153-166.
- 733 4. Nho, E. Y.; Ardouin, B.; Le Cloarec, M. F.; Ramonet, M., Origins of ^{210}Po in the atmosphere
734 at Lamto, Ivory Coast: Biomass burning and Saharan dusts. *Atmos. Environ.* **1996**, *30*, (22),
735 3705-3714.
- 736 5. Carvalho, F. P.; Oliveira, J. M.; Malta, M., Exposure to radionuclides in smoke from
737 vegetation fires. *Sci. Total Environ.* **2014**, *472*, 421-424.
- 738 6. Kashparov, V. A.; Zhurba, M. A.; Zibtsev, S. V.; Mironyuk, V. V.; Kireev, S. I., Evaluation
739 of the expected doses of fire brigades at the Chernobyl exclusion zone in April 2015 [in
740 Russian]. *Nuclear Physics and Atomic Energy* **2015**, *16*, (4), 399-407.
- 741 7. Amiro, B. D.; Sheppard, S. C.; Johnston, F. L.; Evenden, W. G.; Harris, D. R., Burning
742 radionuclide question: What happens to iodine, cesium and chlorine in biomass fires? *Sci.*
743 *Total Environ.* **1996**, *187*, (2), 93-103.
- 744 8. Dusha-Gudym, S. I., Forest fires on areas contaminated by radionuclides from the Chernobyl
745 power plant accident. *Int. Forest Fire News* **1992**, *7*, 4.

- 746 9. Dusha-Gudym, S. I., *The Effects of Forest Fires on the Concentration and Transport of*
747 *Radionuclides. Fire in Ecosystems of Boreal Eurasia*. Kluwer Academic Publishers:
748 Dordrecht, 1996; Vol. 48.
- 749 10. Dusha-Gudym, S. I., Transport of radioactive materials by wildland fires in the Chernobyl
750 Accident zone: How to address the problem. *Int. Forest Fire News* **2005**, 119-125.
- 751 11. Kaletnik, N. N., *Fire prevention and detection in closed zone*. In: "*Fire prevention, liquidation*
752 *and impacts on the lands polluted by radionuclides*". Forestry Institute of the National
753 Academy of Sciences: Gomel, 2002; Vol. 54.
- 754 12. Paatero, J.; Vesterbacka, K.; Makkonen, U.; Kyllönen, K.; Hellen, H.; Hatakka, J.; Anttila, P.,
755 Resuspension of radionuclides into the atmosphere due to forest fires. *J. Radioanal. Nucl.*
756 *Chem.* **2009**, 282, (2), 473-476.
- 757 13. Lujaniene, G.; Šapolaite, J.; Remeikis, V.; Lujanas, V.; Jermolajev, A.; Aninkevičius, V.,
758 Cesium, americium and plutonium isotopes in ground level air of Vilnius. *Czech. J. Phys.*
759 **2006**, 56, (4), D55-D61.
- 760 14. Usenia, V. V.; Yurievich, N. N., The experience of Belarus in forest fire suppression [in
761 Russian]. *Sustainable Forest Management* **2017**, 2, 14-21.
- 762 15. Kovalets, I.; De With, G., Wildfires in the Chernobyl exclusion zone – a summary of the 2020
763 event. *Dutch Magazine for Radiation Protection* **2020**, 11, 31-36.
- 764 16. Allard, G., Fire prevention in radiation-contaminated forests. *Unasylva* **2001**, 52, (207), 41-
765 42.
- 766 17. Ager, A. A.; Lasko, R.; Myroniuk, V.; Zibtsev, S.; Day, M. A.; Usenia, U.; Bogomolov, V.;
767 Kovalets, I.; Evers, C. R., The wildfire problem in areas contaminated by the Chernobyl
768 disaster. *Sci. Total Environ.* **2019**, 696, 133954.
- 769 18. Smith, J. T.; Beresford, N. A., *Chernobyl - Catastrophe and Consequences*. Springer-Praxis
770 Publishing: Chichester, 2005; p 327.
- 771 19. Strode, S. A.; Ott, L. E.; Pawson, S.; Bowyer, T. W., Emission and transport of cesium-137
772 from boreal biomass burning in the summer of 2010. *J. Geophys. Res.: Atmos.* **2012**, 117, (D9).
- 773 20. Sorokina, L. Y.; Petrov, M. F., Changes in the structure of the land cover and fire safety of the
774 Chernobyl exclusion zone landscapes: Assessment methods using satellites. *Ukrainian*
775 *Geographical Journal* **2020**, 45-56.
- 776 21. Protsak, V. P.; Wojciechowicz, O. V.; Laptev, G. V. Estimation of radioactive source term
777 dynamics for atmospheric transport during wildfires in Chernobyl Zone in Spring 2020.
778 <https://uhmi.org.ua/msg/fire2020/analytical.pdf> (accessed March 2021).
- 779 22. Masson, O.; Piga, D.; Le Roux, G.; Mary, J.; de Vismes, A.; Gurriaran, R.; Renaud, P.; Saey,
780 L.; Paulat, P., Recent trends and explanation for airborne ¹³⁷Cs activity level increases in
781 France. *Radioprotection* **2009**, 44, (2), 327-332.
- 782 23. SCK-CEN 1 [https://www.sckcen.be/sites/default/files/files/2020-](https://www.sckcen.be/sites/default/files/files/2020-04/Forest%20fires%20Chernobyl_Radiological%20follow%20up_20200415.pdf)
783 [04/Forest%20fires%20Chernobyl_Radiological%20follow%20up_20200415.pdf](https://www.sckcen.be/sites/default/files/files/2020-04/Forest%20fires%20Chernobyl_Radiological%20follow%20up_20200415.pdf) (Accessed
784 December 2020).
- 785 24. SCK-CEN 2 [https://www.sckcen.be/sites/default/files/files/2020-](https://www.sckcen.be/sites/default/files/files/2020-04/Forest%20fires%20Chernobyl_Radiological%20follow%20up_20200430_1.pdf)
786 [04/Forest%20fires%20Chernobyl_Radiological%20follow%20up_20200430_1.pdf](https://www.sckcen.be/sites/default/files/files/2020-04/Forest%20fires%20Chernobyl_Radiological%20follow%20up_20200430_1.pdf)
787 (Accessed December 2020).

- 788 25. IRSN 1 [https://www.irsn.fr/EN/newsroom/News/Pages/20200415_Fires-in-Ukraine-in-the-](https://www.irsn.fr/EN/newsroom/News/Pages/20200415_Fires-in-Ukraine-in-the-Exclusion-Zone-around-chernobyl.aspx)
789 [Exclusion-Zone-around-chernobyl.aspx](https://www.irsn.fr/EN/newsroom/News/Pages/20200415_Fires-in-Ukraine-in-the-Exclusion-Zone-around-chernobyl.aspx) (Accessed December 2020).
- 790 26. IRSN 2 [https://www.irsn.fr/EN/newsroom/News/Pages/20200420_Fires-in-Ukraine-in-the-](https://www.irsn.fr/EN/newsroom/News/Pages/20200420_Fires-in-Ukraine-in-the-Exclusion-Zone-around-chernobyl.aspx)
791 [Exclusion-Zone-around-chernobyl.aspx](https://www.irsn.fr/EN/newsroom/News/Pages/20200420_Fires-in-Ukraine-in-the-Exclusion-Zone-around-chernobyl.aspx) (Accessed 2020).
- 792 27. IRSN 3 [https://www.irsn.fr/EN/newsroom/News/Pages/20200424_Fires-in-Ukraine-in-the-](https://www.irsn.fr/EN/newsroom/News/Pages/20200424_Fires-in-Ukraine-in-the-Exclusion-Zone-around-chernobyl-cesium-137-results-in-france.aspx)
793 [Exclusion-Zone-around-chernobyl-cesium-137-results-in-france.aspx](https://www.irsn.fr/EN/newsroom/News/Pages/20200424_Fires-in-Ukraine-in-the-Exclusion-Zone-around-chernobyl-cesium-137-results-in-france.aspx) (Accessed December
794 2020).
- 795 28. IRSN 4 [https://www.irsn.fr/EN/newsroom/News/Pages/20200505_Fires-in-Ukraine-in-the-](https://www.irsn.fr/EN/newsroom/News/Pages/20200505_Fires-in-Ukraine-in-the-Exclusion-Zone-around-chernobyl-latest-news-and-consequences.aspx)
796 [Exclusion-Zone-around-chernobyl-latest-news-and-consequences.aspx](https://www.irsn.fr/EN/newsroom/News/Pages/20200505_Fires-in-Ukraine-in-the-Exclusion-Zone-around-chernobyl-latest-news-and-consequences.aspx) (Accessed December
797 2020).
- 798 29. UNSCEAR, *Exposures and effects of the Chernobyl accident (Annex J)*. United Nations: New
799 York, 2000.
- 800 30. Tabachnyi, L.; Kokot, I., *Results of consequences of the fires on the radioactive contamination*
801 *territories of Kyiv and Zhytomyr regions according to Hydrometeorological radiometrical*
802 *network data*. IAEA: Vienna, 2020.
- 803 31. Pazukhin, E. M.; Borovoi, A. A.; Ogorodnikov, B. I., Forest Fire as a Factor of Environmental
804 Redistribution of Radionuclides Originating from Chernobyl Accident. *Radiochemistry* **2004**,
805 *46*, (1), 102-106.
- 806 32. Yoschenko, V. I.; Kashparov, V. A.; Protsak, V. P.; Lundin, S. M.; Levchuk, S. E.; Kadygrib,
807 A. M.; Zvarich, S. I.; Khomutinin, Y. V.; Maloshtan, I. M.; Lanshin, V. P.; Kovtun, M. V.;
808 Tschiersch, J., Resuspension and redistribution of radionuclides during grassland and forest
809 fires in the Chernobyl exclusion zone: part I. Fire experiments. *J. Environ. Radioact.* **2006**, *86*,
810 (2), 143-163.
- 811 33. Steinhauser, G., Anthropogenic radioactive particles in the environment. *J. Radioanal. Nucl.*
812 *Chem.* **2018**, *318*, (3), 1629-1639.
- 813 34. IAEA, *Environmental consequences of the Chernobyl accident and their remediation: twenty*
814 *years of experience. Radiological assessment reports series*. IAEA: Vienna, 2006.
- 815 35. Blake, N. J.; Blake, D. R.; Wingenter, O. W.; Sive, B. C.; McKenzie, L. M.; Lopez, J. P.;
816 Simpson, I. J.; Fuelberg, H. E.; Sachse, G. W.; Anderson, B. E.; Gregory, G. L.; Carroll, M.
817 A.; Albercook, G. M.; Rowland, F. S., Influence of southern hemispheric biomass burning on
818 midtropospheric distributions of nonmethane hydrocarbons and selected halocarbons over the
819 remote South Pacific. *J. Geophys. Res.: Atmos.* **1999**, *104*, (D13), 16213-16232.
- 820 36. Jargin, S. V., Forest fires in the former Soviet Union: no reasons for radiophobia. *J. Environ.*
821 *Radioact.* **2011**, *102*, (2), 218-219.
- 822 37. Kashparov, V. A.; Lundin, S. M.; Khomutinin, Y. V.; Kaminsky, S. P.; Levchuk, S. E.;
823 Protsak, V. P.; Kadygrib, A. M.; Zvarich, S. I.; Yoschenko, V. I.; Tschiersch, J., Soil
824 contamination with Sr-90 in the near zone of the Chernobyl accident. *J. Environ. Radioact.*
825 **2001**, *56*, (3), 285-298.
- 826 38. Evangelidou, N.; Eckhardt, S., Uncovering transport, deposition and impact of radionuclides
827 released after the early spring 2020 wildfires in the Chernobyl Exclusion Zone. *Sci. Rep.* **2020**,
828 *10*, (1), 10655.
- 829 39. State Nuclear Regulatory Inspectorate of Ukraine
830 <http://www.snrc.gov.ua/nuclear/en/publish/article/368134> (Accessed December 2020).

- 831 40. Kirieiev, S. Estimation and forecast of the impact on the radiation situation of extreme natural
832 factors flood, wildfire, etc. [http://dazv.gov.ua/images/pdf/ukraino-japonskyj-](http://dazv.gov.ua/images/pdf/ukraino-japonskyj-komitet/fifth/Sergii%20KIRIEEV.pdf)
833 [komitet/fifth/Sergii%20KIRIEEV.pdf](http://dazv.gov.ua/images/pdf/ukraino-japonskyj-komitet/fifth/Sergii%20KIRIEEV.pdf) (Accessed December 2020).
- 834 41. Holiaka, D.; Yoschenko, V.; Levchuk, S.; Kashparov, V., Distributions of ^{137}Cs and ^{90}Sr
835 activity concentrations in trunk of Scots pine (*Pinus sylvestris* L.) in the Chernobyl zone. *J.*
836 *Environ. Radioact.* **2020**, *222*, 106319.
- 837 42. AEN-OCDE, *Tchernobyl. Evaluation de l'impact radiologique et sanitaire. Mise à jour de*
838 *2002 de «Tchernobyl Dix ans déjà »*. Agence pour l'énergie nucléaire, Organisation de
839 coopération et de développement économiques. Les éditions de l'OCDE: Paris, 2002; p 35-37.
- 840 43. Holm, E.; Rioseco, J.; Pettersson, H., Fallout of transuranium elements following the
841 Chernobyl accident. *J. Radioanal. Nucl. Chem.* **1992**, *156*, (1), 183-200.
- 842 44. Kashparov, V. A.; Lundin, S. M.; Zvarych, S. I.; Yoshchenko, V. I.; Levchuk, S. E.;
843 Khomutinin, Y. V.; Maloshtan, I. M.; Protsak, V. P., Territory contamination with the
844 radionuclides representing the fuel component of Chernobyl fallout. *Sci. Total Environ.* **2003**,
845 *317*, (1-3), 105-119.
- 846 45. Ministry of Health of Ukraine, *Radiation Safety Standards of Ukraine. NRBU-97/D-2000.*
847 Ministry of Health of Ukraine: Kyiv, 2000.
- 848 46. Ovadnevaitė, J.; Kvietkus, K.; Maršalka, A., 2002 summer fires in Lithuania: Impact on the
849 Vilnius city air quality and the inhabitants health. *Sci. Total Environ.* **2006**, *356*, (1), 11-21.
- 850 47. Stoulos, S.; Basis, A.; Ioannidou, A., Determination of low ^{137}Cs concentration in the
851 atmosphere due to Chernobyl contaminated forest-wood burning. *J. Environ. Radioact.* **2020**,
852 *222*, 106383.
- 853 48. Muramatsu, Y.; Rühm, W.; Yoshida, S.; Tagami, K.; Uchida, S.; Wirth, E., Concentrations of
854 ^{239}Pu and ^{240}Pu and Their Isotopic Ratios Determined by ICP-MS in Soils Collected from the
855 Chernobyl 30-km Zone. *Environ. Sci. Technol.* **2000**, *34*, (14), 2913-2917.
- 856 49. Talerko, M.; Kovalets, I.; Lev, T.; Igarashi, Y.; Romanenko, O., Simulation study of
857 radionuclide atmospheric transport after wildland fires in the Chernobyl Exclusion Zone in
858 April 2020. *Atmospheric Pollution Research* **2021**, *12*, (3), 193-204.
- 859 50. De Meutter, P.; Gueibe, C.; Tomas, J.; Outer, P. d.; Apituley, A.; Bruggeman, M.; Camps, J.;
860 Delcloo, A.; Knetsch, G.-J.; Roobol, L.; Verheyen, L., The assessment of the April 2020
861 Chernobyl wildfires and their impact on Cs-137 levels in Belgium and The Netherlands. *J.*
862 *Environ. Radioact.* **2021**, *237*, 106688.
- 863 51. Jakopič, R.; Richter, S.; Kühn, H.; Aregbe, Y., Determination of $^{240}\text{Pu}/^{239}\text{Pu}$, $^{241}\text{Pu}/^{239}\text{Pu}$ and
864 $^{242}\text{Pu}/^{239}\text{Pu}$ isotope ratios in environmental reference materials and samples from Chernobyl
865 by thermal ionization mass spectrometry (TIMS) and filament carburization. *J. Anal. At.*
866 *Spectrom.* **2010**, *25*, (6), 815-821.
- 867 52. Carbol, P.; Solatie, D.; Erdmann, N.; Nylén, T.; Betti, M., Deposition and distribution of
868 Chernobyl fallout fission products and actinides in a Russian soil profile. *J. Environ. Radioact.*
869 **2003**, *68*, (1), 27-46.
- 870 53. Paatero, J.; Jaakkol, T.; Reponen, A., Determination of the ^{241}Pu deposition in Finland after
871 the Chernobyl Accident. *Radiochim. Acta* **1994**, *64*, (2), 139-144.
- 872 54. Mielelski, J. W.; Szwalko, P.; Tomankiewicz, E.; Gaca, P.; Małek, S.; Barszcz, J.; Grabowska,
873 S., ^{137}Cs , ^{40}K , ^{90}Sr , 238 , $^{239+240}\text{Pu}$, ^{241}Am and $^{243+244}\text{Cm}$ in forest litter and their transfer to some

- 874 species of insects and plants in boreal forests: Three case studies. *J. Radioanal. Nucl. Chem.*
875 **2004**, 262, (3), 645-660.
- 876 55. Ketterer, M. E.; Hafer, K. M.; Mietelski, J. W., Resolving Chernobyl vs. global fallout
877 contributions in soils from Poland using Plutonium atom ratios measured by inductively
878 coupled plasma mass spectrometry. *J. Environ. Radioact.* **2004**, 73, (2), 183-201.
- 879 56. Salminen-Paatero, S.; Paatero, J.; Jaakkola, T., ^{241}Pu and $^{241}\text{Pu}/^{239+240}\text{Pu}$ activity ratio in
880 environmental samples from Finland as evaluated by the ingrowth of ^{241}Am . *Boreal Environ.*
881 *Res.* **2014**, 19, 51-65.
- 882 57. Vukanac, I.; Paligorić, D.; Novković, D.; Djurašević, M.; Obradović, Z.; Milošević, Z.; Manić,
883 S., Retrospective estimation of the concentration of ^{241}Pu in air sampled at a Belgrade site
884 following the Chernobyl accident. *Appl. Radiat. Isot.* **2006**, 64, (6), 689-692.
- 885 58. Sokolik, G. A.; Ovsiannikova, S. V.; Ivanova, T. G.; Leinova, S. L., Soil-plant transfer of
886 plutonium and americium in contaminated regions of Belarus after the Chernobyl catastrophe.
887 *Environ. Int.* **2004**, 30, (7), 939-947.
- 888 59. Lehto, J.; Vaaramaa, K.; Leskinen, A., ^{137}Cs , $^{239,240}\text{Pu}$ and ^{241}Am in boreal forest soil and their
889 transfer into wild mushrooms and berries. *J. Environ. Radioact.* **2013**, 116, 124-132.
- 890 60. Zheng, J.; Tagami, K.; Watanabe, Y.; Uchida, S.; Aono, T.; Ishii, N.; Yoshida, S.; Kubota, Y.;
891 Fuma, S.; Ihara, S., Isotopic evidence of plutonium release into the environment from the
892 Fukushima DNPP accident. *Sci. Rep.* **2012**, 2, 304.
- 893 61. Nisbet, A. F.; Shaw, S., Summary of a 5-year lysimeter study on the time-dependent transfer
894 of ^{137}Cs , ^{90}Sr , $^{239,240}\text{Pu}$ and ^{241}Am to crops from three contrasting soil types: 1. Transfer to the
895 edible portion. *J. Environ. Radioact.* **1994**, 23, (1), 1-17.
- 896 62. Dvornik, A. A.; Dvornik, A. M.; Korol, R. A.; Shamal, N. V.; Gaponenko, S. O.; Bardyukova,
897 A. V., Potential threat to human health during forest fires in the Belarusian exclusion zone.
898 *Aerosol Sci. Technol.* **2018**, 52, (8), 923-932.
- 899 63. Buzdalkin, K. N.; Bortnovsky, V. N., *Inhalation of transuranic elements in case of*
900 *emergencies in the exclusion zone of the Chernobyl NPP. Medico-Biological and Socio-*
901 *Psychological Issues of Safety in Emergency Situations (in Russian)*. Nikiforov Russian Center
902 of Emergency and Radiation Medicine, EMERCOM of Russia: 2019.
- 903 64. Security, R. N. [http://russiannuclearsecurity.com/wildfires-in-ukraine-draw-dangerously-](http://russiannuclearsecurity.com/wildfires-in-ukraine-draw-dangerously-close-to-chernobyl-exclusion-zone)
904 [close-to-chernobyl-exclusion-zone](http://russiannuclearsecurity.com/wildfires-in-ukraine-draw-dangerously-close-to-chernobyl-exclusion-zone) (Accessed December 2020).
- 905 65. Antropov, V. M.; Bugai, D. A.; Dutton, L. M.; Gerchikov, M. Y.; Kennett, E. J.; Ledenev, A.
906 I.; Novikov, A. A.; Rudko, V.; Ziegenhagen, J., *Review and analysis of solid long-lived and*
907 *high level radioactive waste arising at the Chernobyl nuclear power plant and the restricted*
908 *zone*. European Commission: 2001.
- 909 66. Shcheglov, A.; Tsvetnova, O. g.; Klyashtorin, A., Biogeochemical cycles of Chernobyl-born
910 radionuclides in the contaminated forest ecosystems. Long-term dynamics of the migration
911 processes. *J. Geochem. Explor.* **2014**, 144, 260-266.
- 912 67. Thiry, Y.; Colle, C.; Yoschenko, V.; Levchuk, S.; Van Hees, M.; Hurtevent, P.; Kashparov,
913 V., Impact of Scots pine (*Pinus sylvestris* L.) plantings on long term ^{137}Cs and ^{90}Sr recycling
914 from a waste burial site in the Chernobyl Red Forest. *J. Environ. Radioact.* **2009**, 100, (12),
915 1062-1068.
- 916 68. Kashparov, V.; Salbu, B.; Simonucci, C.; Levchuk, S.; Reinoso-Maset, E.; Lind, O. C.;
917 Maloshtan, I.; Protsak, V.; Courbet, C.; Nguyen, H., Validation of a fuel particle dissolution

918 model with samples from the Red Forest within the Chernobyl exclusion zone. *J. Environ.*
919 *Radioact.* **2020**, 223-224, 106387.

920 69. Kashparov, V.; Salbu, B.; Levchuk, S.; Protsak, V.; Maloshtan, I.; Simonucci, C.; Courbet, C.;
921 Nguyen, H. L.; Sanzharova, N.; Zabrotsky, V., Environmental behaviour of radioactive
922 particles from Chernobyl. *J. Environ. Radioact.* **2019**, 208-209, 106025.

923 70. ICRP 66, Human Respiratory Tract Model for Radiological Protection. *ICRP Publication*
924 **1994**, 66.

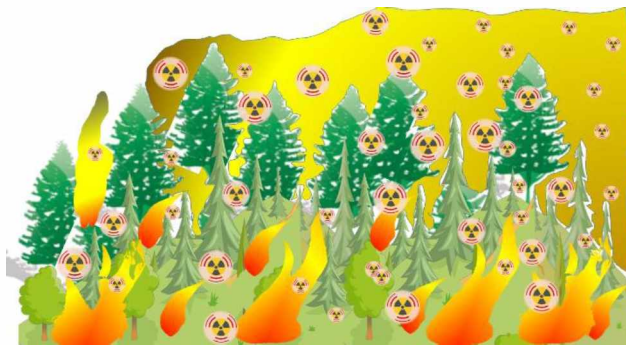
925 71. ICRP 119, Compendium of Dose Coefficients based on ICRP Publication 60. *Ann. ICRP* **2012**,
926 *41*, 1-130.

927 72. ICRP 71, Age-dependent Doses to Members of the Public from Intake of Radionuclides. Part
928 4. Inhalation Dose Coefficients. *ICRP Publication* **1995**, 71.

929 73. 134, I., Occupational Intakes of Radionuclides: Part 2. *Ann. ICRP* **2016**, 45, 1-352.

930 74. Terray, L.; D'Amico, D.; Masson, O.; Sabroux, J.-C., What can gross alpha/beta activities tell
931 about ^{210}Po and ^{210}Pb in the atmosphere? *J. Environ. Radioact.* **2020**, 225, 106437.

932
933
934
935
936
937
938
939
940



941
942

For Table of Contents only